Astron. Astrophys. 270, 204–222 (1993)

ASTRONOMY AND ASTROPHYSICS

Monitoring of very rapid changes in the optical spectrum of SS 433 in May/June 1987

R.C. Vermeulen[1,*], P.G. Murdin[2,], E.P.J. van den Heuvel[3], S.N. Fabrika[4], R.M. Wagner[5], B. Margon[6], J.B. Hutchings[7], R.T. Schilizzi[8], M.H. van Kerkwijk[3], L.B. van den Hoek[3], E. Ott[3], L.P. Angebault[9], G.K. Miley[1], S. D'Odorico[9], and N. Borisov[4]**

[1] Leiden Observatory, P.O. Box 9513, NL-2300 RA, Leiden, The Netherlands
[2] Royal Greenwich Observatory, Madingley Road, Cambridge, CB3 0EZ, Britain
[3] Astronomical Institute, University of Amsterdam, Kruislaan 403, NL-1098 SJ, Amsterdam, The Netherlands
[4] Special Astrophysical Observatory AS USSR, Nizhnij Arkhyz, Stavropol Territory, 357147, Russia
[5] Department of Astronomy, The Ohio State University, Columbus, OH 43210, USA
[6] Department of Astronomy, University of Washington, Seattle, WA 98195, USA
[7] Dominion Astrophysical Observatory, 5071 W. Saanich Road, Victoria, BC V8X 4M6, Canada
[8] Netherlands Foundation for Research in Astronomy, P.O. Box 2, NL-7990 AA, Dwingeloo, The Netherlands
[9] European Southern Observatory, Karl Schwarzschildstraße 2, W-8046 Garching bei München, Germany

Received July 7, accepted November 18, 1992

Abstract. Intensive spectroscopic monitoring of SS 433 was undertaken in May/June of 1987 as part of a multi-wavelength campaign. The evolution of the moving emission lines from the jets was followed for several weeks on timescales of hours. Their properties can be described in terms of "bullets", or discrete line components. These components are not correlated on a one-to-one basis between the approaching and the receding jet. However, the statistical properties in the two jets are the same after compensation for orientation effects, and extreme events, such as a temporary absence of moving line emission, are correlated. The bullets are found to have reasonably well-defined parameters. Typical or preferred values are derived for the line width ($\sim$1700 km s^{-1}), the maximum equivalent width ($\sim$25 Å at 6797 Å), and the time taken to reach that maximum ($\sim$10 hours). The total radiative lifetime is typically $\sim$2 days; some bullets persist for up to 6 days. The bullet generation interval is typically $<$1 day. Hence more than one line component is usually visible in the spectrum at any given time. There is evidence that at least some bullets may be composed of smaller entities. Models need to be developed to explain the contrast between the clumpiness of the jets as seen in optical line emission, and the more continuous outflow suggested by X-ray and radio emission; two-phase jets with varying amounts of cool dense matter embedded in a hot and more continuous medium seem attractive.

The complexity of the so-called stationary line emission is also discussed. The Balmer and Paschen lines show evidence for double peaks; additionally they have broad wings. The properties of the hydrogen lines are more akin to those of He II λ4686 than was once thought. However, doubt is cast on an interpretation in terms of Keplerian rotation in an accretion disk. Only the blue peak in H_α shows evidence for eclipses, and the red peak, which can be most easily tracked, does not display significant orbital radial velocity variations. Outflow phenomena from the SS 433 binary system as a whole may well be involved. On the other hand, the centroid of H_α does show an orbital radial velocity curve, indicating that at least part of the emission originates near the compact object. Given the complex origin which is likely for both the hydrogen lines and for He II λ4686, all values derived for the Doppler amplitude (K) should be interpreted with great caution.

Key words: SS 433 – spectroscopy – line profiles – jets – binaries: eclipsing – astronomical databases: miscellaneous

1. Introduction

An intensive multi-wavelength monitoring campaign on SS 433 was carried out in May/June 1987. In this paper the resultant unique database of optical spectra is presented. Using 10 different telescopes, 178 spectra were obtained in less than 14 days, and 202 spectra were observed in total within 24 days. The primary goal was to track the evolution of the moving H_α lines at fairly high resolution, but the total spectral coverage obtained runs from 3300 to 9760 Å. Reports on other aspects of the

Send offprint requests to: R.C. Vermeulen
* Present address: Owens Valley Radio Observatory 105-24, California Institute of Technology, Pasadena, CA 91125, USA
** Present address: Royal Observatory, Blackford Hill, Edinburgh EH9 3HJ, Scotland, Britain

Table 1. Overview of the spectral database. For each spectrum, we list the Julian Date for the midpoint of the observation, the wavelength range, the observatory, the integration time, and the resolution. Observatory codes are as follows: 6M = USSR 6 m; C1 = Calar Alto 1.2 m; C2 = Calar Alto 2.2 m; DO = Dominion 1.9 m; FS = Flagstaff 1.8 m; KP = Kitt Peak 0.9 m; LI = Lick 3 m; LP = La Palma 2.5 m; LS = La Silla 1.5 m; PA = Palomar 5 m

JD−2440000	Wav. range Å	Tel.	Int. time (sec)	Resol. Å	JD−2440000	Wav. range Å	Tel.	Int. time (sec)	Resol. Å
6933.997	6048 – 8491	PA	200	6.0	6940.632	3934 – 7898	LP	1750	3.2
6934.967	6048 – 8491	PA	200	6.0	6940.632	4100 – 6670	C1	899	3.0
6935.424	5300 – 6323	6M	1313	1.5	6940.827	5520 – 8120	FS	2400	10.0
6935.513	4100 – 6670	C1	1801	3.0	6940.892	3720 – 6339	FS	3600	10.0
6935.582	4100 – 6670	C1	5469	3.0	6940.931	5520 – 8120	FS	1800	10.0
6936.490	4100 – 6670	C1	3363	3.0	6940.933	3300 – 7039	DO	470	8.0
6936.597	4100 – 6670	C1	1985	3.0	6940.942	3300 – 7039	DO	820	8.0
6936.652	5760 – 6700	LP	371	0.8	6941.534	4100 – 6670	C1	3601	3.0
6936.657	5760 – 6700	LP	400	0.8	6941.634	4100 – 6670	C1	3602	3.0
6936.666	5760 – 6700	LP	700	0.8	6941.660	5776 – 7760	LP	213	1.6
6936.682	7010 – 7950	LP	1500	0.8	6941.925	5435 – 6603	LS	1971	2.5
6936.714	5760 – 6700	LP	1500	0.8	6941.944	4200 – 5434	DO	1399	2.0
6936.792	6325 – 8795	LS	900	5.0	6941.945	6500 – 7698	LS	850	2.5
6936.803	6325 – 8795	LS	900	5.0	6942.474	4100 – 6670	C1	712	3.0
6936.875	5440 – 7970	LS	1200	5.0	6942.594	7010 – 7950	LP	1050	0.8
6936.890	5440 – 7970	LS	1200	5.0	6942.606	7010 – 7950	LP	1000	0.8
6936.908	5440 – 7970	LS	1850	5.0	6942.628	5760 – 6700	LP	700	0.8
6936.952	4300 – 6791	DO	900	4.0	6942.638	5760 – 6700	LP	700	0.8
6936.961	4400 – 6891	DO	1000	4.0	6942.645	4100 – 6670	C1	2847	3.0
6937.519	4100 – 6670	C1	3602	3.0	6942.656	3916 – 4856	LP	1400	0.8
6937.633	4100 – 6670	C1	3603	3.0	6942.676	4808 – 5748	LP	1000	0.8
6937.661	5760 – 6700	LP	1051	0.8	6942.715	6390 – 7330	LP	600	0.8
6937.682	7010 – 7950	LP	2000	0.8	6942.727	5760 – 6700	LP	500	0.8
6937.731	5760 – 6700	LP	400	0.8	6942.794	5520 – 8120	FS	2400	10.0
6937.937	4500 – 6991	DO	1000	4.0	6942.837	3720 – 6339	FS	3600	10.0
6937.951	4500 – 6991	DO	1068	4.0	6942.879	5520 – 8120	FS	2400	10.0
6938.654	5760 – 6700	LP	500	0.8	6942.926	5520 – 8120	FS	1200	10.0
6938.663	5760 – 6700	LP	900	0.8	6942.968	3640 – 6901	KP	600	10.0
6938.685	7010 – 7950	LP	2400	0.8	6943.561	7010 – 7950	LP	1200	0.8
6938.734	6390 – 7330	LP	627	0.8	6943.578	5760 – 6700	LP	600	0.8
6938.818	5520 – 8120	FS	1800	10.0	6943.587	5760 – 6700	LP	600	0.8
6938.868	5520 – 8120	FS	1800	10.0	6943.593	5760 – 6700	LP	400	0.8
6938.896	5520 – 8120	FS	1800	10.0	6943.598	5760 – 6700	LP	400	0.8
6938.930	5520 – 8120	FS	1330	10.0	6943.604	5760 – 6700	LP	400	0.8
6939.510	5350 – 6373	6M	3416	1.5	6943.611	5760 – 6700	LP	400	0.8
6939.658	5760 – 6700	LP	1200	0.8	6943.617	5760 – 6700	LP	400	0.8
6939.678	7010 – 7950	LP	1474	0.8	6943.632	7010 – 7950	LP	1100	0.8
6939.701	7010 – 7950	LP	1000	0.8	6943.642	7010 – 7950	LP	600	0.8
6939.714	6390 – 7330	LP	1000	0.8	6943.648	7010 – 7950	LP	210	0.8
6939.782	5435 – 6604	LS	1800	2.5	6943.655	7010 – 7950	LP	600	0.8
6939.802	5520 – 8120	FS	2400	10.0	6943.662	7010 – 7950	LP	600	0.8
6939.813	5435 – 6604	LS	2400	2.5	6943.670	7010 – 7950	LP	600	0.8
6939.831	5520 – 8120	FS	1800	10.0	6943.678	7010 – 7950	LP	600	0.8
6939.855	6558 – 7727	LS	1800	2.5	6943.690	7010 – 7950	LP	600	0.8
6939.888	3720 – 6339	FS	3000	10.0	6943.697	7010 – 7950	LP	600	0.8
6939.895	3300 – 7039	DO	750	8.0	6943.705	7010 – 7950	LP	600	0.8
6939.896	6558 – 7727	LS	2400	2.5	6943.725	5760 – 6700	LP	518	0.8
6939.905	3300 – 7039	DO	850	8.0	6943.731	7010 – 7950	LP	400	0.8
6939.938	5520 – 8120	FS	4200	10.0	6943.963	3640 – 6901	KP	600	10.0
6940.492	4100 – 6670	C1	3602	3.0	6944.456	4100 – 6670	C1	3613	3.0
6940.576	4100 – 6670	C1	3602	3.0	6944.523	4100 – 6670	C1	3603	3.0

Table 1. (continued)

JD−2440000	Wav. range Å	Tel.	Int. time (sec)	Resol. Å	JD−2440000	Wav. range Å	Tel.	Int. time (sec)	Resol. Å
6944.611	4100 – 6670	C1	3602	3.0	6947.704	6302 – 7366	LP	1000	0.8
6944.627	5682 – 6746	LP	300	0.8	6947.719	7684 – 8748	LP	900	0.8
6944.631	5682 – 6746	LP	403	0.8	6947.947	5192 – 8387	LI	600	10.0
6944.640	5682 – 6746	LP	800	0.8	6948.479	4100 – 6670	C1	3602	3.0
6944.657	6932 – 7996	LP	1000	0.8	6948.608	4100 – 6670	C1	3963	3.0
6944.669	6932 – 7996	LP	1000	0.8	6948.624	4850 – 6750	C2	2400	1.0
6944.708	6302 – 7366	LP	1000	0.8	6948.651	5956 – 6578	LP	200	1.2
6944.721	6932 – 7996	LP	539	0.8	6948.660	6098 – 6720	LP	500	1.2
6944.958	3640 – 6901	KP	600	10.0	6948.671	7194 – 7816	LP	500	1.2
6945.385	5340 – 6363	6M	1146	1.5	6948.691	6098 – 6720	LP	500	1.2
6945.506	4100 – 6670	C1	3602	3.0	6948.698	7194 – 7816	LP	500	1.2
6945.605	4050 – 5850	C2	3000	1.0	6948.706	6098 – 6720	LP	400	1.2
6945.629	5682 – 6746	LP	430	0.8	6948.713	7194 – 7816	LP	400	1.2
6945.635	5682 – 6746	LP	430	0.8	6948.722	7860 – 8482	LP	400	1.2
6945.641	5682 – 6746	LP	430	0.8	6948.729	8512 – 9134	LP	400	1.2
6945.649	4100 – 6670	C1	2401	3.0	6948.737	9154 – 9776	LP	400	1.2
6945.656	6932 – 7996	LP	1000	0.8	6948.875	4200 – 5434	DO	1755	2.0
6945.668	6932 – 7996	LP	1000	0.8	6948.938	4200 – 5434	DO	1423	2.0
6945.696	6302 – 7366	LP	1000	0.8	6949.472	5430 – 6453	6M	1839	1.5
6945.711	5682 – 6746	LP	600	0.8	6949.518	4100 – 6670	C1	3602	3.0
6945.720	6932 – 7996	LP	810	0.8	6949.623	4850 – 6750	C2	2400	1.0
6945.960	3640 – 6901	KP	600	10.0	6949.648	6106 – 6522	LP	500	0.8
6945.983	5220 – 8384	LI	300	10.0	6949.655	6496 – 6914	LP	500	0.8
6946.488	5340 – 6363	6M	1429	1.5	6949.665	7276 – 7694	LP	500	0.8
6946.494	4100 – 6670	C1	3603	3.0	6949.688	8052 – 8470	LP	500	0.8
6946.552	4850 – 6750	C2	3168	1.0	6949.697	8442 – 8860	LP	600	0.8
6946.602	4100 – 6670	C1	3602	3.0	6949.707	7666 – 8084	LP	600	0.8
6946.633	5506 – 6672	LS	556	2.5	6949.719	5326 – 5744	LP	1000	0.8
6946.635	5682 – 6746	LP	400	0.8	6949.733	8836 – 9254	LP	700	0.8
6946.640	5682 – 6746	LP	400	0.8	6949.936	4200 – 5434	DO	1001	2.0
6946.646	5682 – 6746	LP	400	0.8	6950.427	5420 – 6443	6M	1946	1.5
6946.651	5506 – 6672	LS	1800	0.8	6950.491	4100 – 6670	C1	3602	3.0
6946.657	6932 – 7996	LP	500	0.8	6950.581	4100 – 6670	C1	3602	3.0
6946.663	6932 – 7996	LP	500	0.8	6951.424	5730 – 6753	6M	2462	1.5
6946.669	6932 – 7996	LP	500	0.8	6951.485	4980 – 6003	6M	6161	1.5
6946.676	6932 – 7996	LP	500	0.8	6951.502	4100 – 6670	C1	3603	3.0
6946.700	6302 – 7366	LP	1000	0.8	6951.580	4100 – 6670	C1	3602	3.0
6946.711	6565 – 7735	LS	1800	2.5	6952.485	4980 – 6003	6M	2608	1.5
6946.715	6932 – 7996	LP	1000	0.8	6952.508	5730 – 6753	6M	1666	1.5
6946.725	7684 – 8748	LP	600	0.8	6952.585	4100 – 6670	C1	4361	3.0
6946.984	3640 – 6901	KP	600	10.0	6953.403	5740 – 6763	6M	3527	1.5
6946.985	5216 – 8383	LI	300	10.0	6953.440	4100 – 6670	C1	2800	3.0
6947.463	4100 – 6670	C1	3602	3.0	6953.454	4310 – 5333	6M	4265	1.5
6947.616	4850 – 6750	C2	1800	1.0	6953.494	4980 – 6003	6M	1782	1.5
6947.639	5682 – 6746	LP	600	0.8	6953.551	4100 – 6670	C1	3602	3.0
6947.651	5682 – 6746	LP	600	0.8	6955.456	4100 – 6670	C1	318	3.0
6947.664	6932 – 7996	LP	500	0.8	6955.630	4100 – 6670	C1	3602	3.0
6947.670	6932 – 7996	LP	500	0.8	6956.581	4100 – 6670	C1	3602	3.0
6947.677	6932 – 7996	LP	500	0.8	6957.431	4100 – 6670	C1	3602	3.0
6947.683	6932 – 7996	LP	500	0.8	6957.521	4100 – 6670	C1	3603	3.0

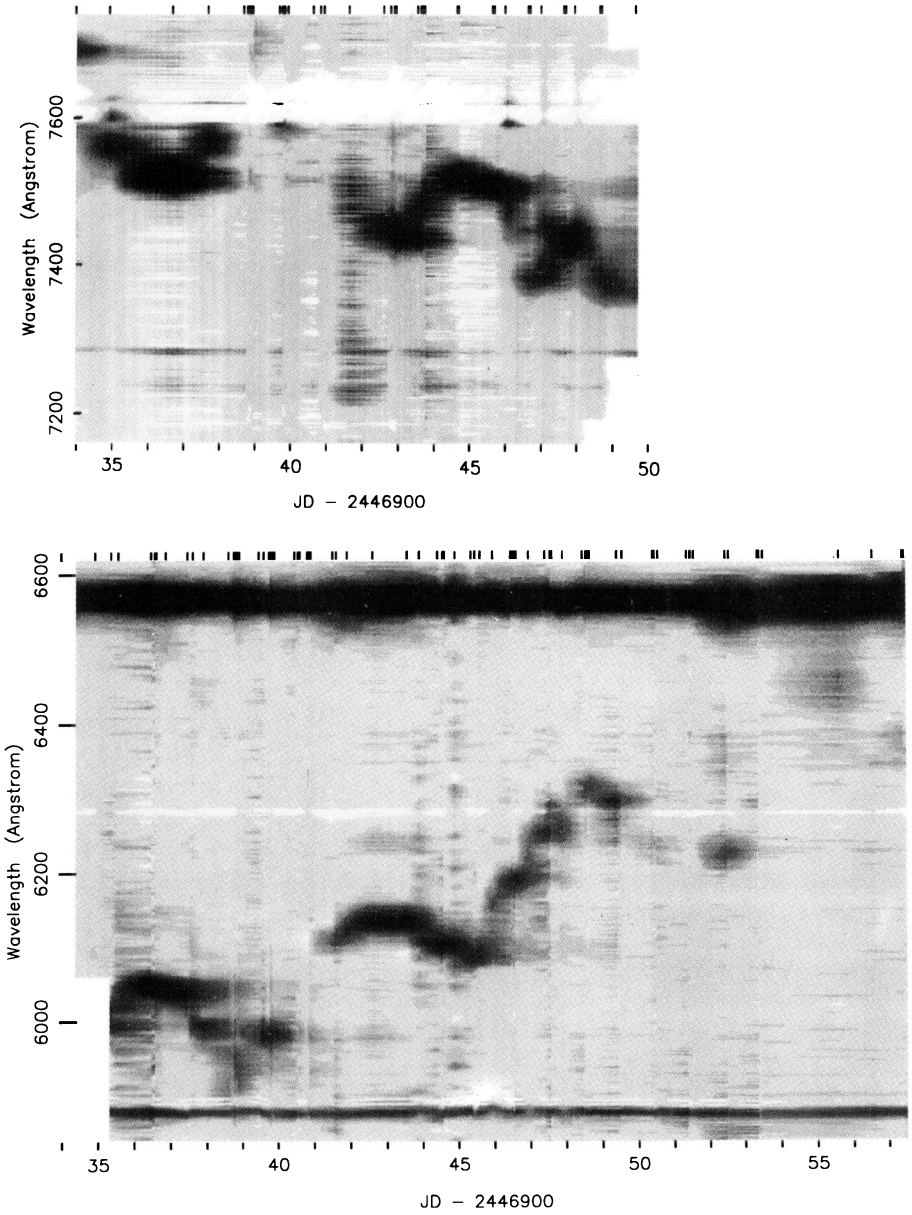

Fig. 1. Grey-scale representation of the full spectral database in the two wavelength ranges covering the moving H_α lines (top: H_α^+, bottom: H_α^-). Time increases horizontally to the right in these diagrams, and wavelength vertically upward. The grey scales have been optimised to show the evolution of the moving H_α lines. All spectra were normalised to a flat continuum value of 1, and the blackest portions of the diagrams indicate the largest peak-to-continuum ratios. The impressive time coverage can be judged from the tick marks at the upper margin, which show the location of all the spectra used to construct these diagrams, as explained in Sect. 2

1987 campaign are given in this issue of Astronomy and Astrophysics by Aslanov et al. (1993), Vermeulen et al. (1993a), and Vermeulen et al. (1993b). Complementary X-ray observations were published by Kawai et al. (1989).

Ever since the discovery of the unique moving Doppler shifted lines (e.g. Margon et al. 1979), the optical spectrum of SS433 has been extensively studied. A summary of the first five years of work, with extensive references, can be found in Margon (1984). SS433 has a heavily reddened continuum ($A_V \approx 8$, e.g. Murdin et al. 1980), which makes it nearly impossible to study the spectrum below $\sim$ 4000 Å. The Balmer series is the most prominent line system in the visible part of the spectrum, while He II λ4686 and C III/N III λ4640–4650 are also present, as well as many lines of He I and Fe II. In the infrared, O I λ8446 and members of the Paschen and Bracket series have been reported. Since these lines are not emitted by matter moving at 0.26c, they have been termed stationary. Many stationary lines have broad, very complex, and variable profiles (e.g. Falomo et al. 1987). This hampers systematic studies of their properties as a function of the well-known periodicities of SS433; different groups have sometimes reached contradictory or puzzling results (compare Anderson et al. 1983, and Asadullaev & Cherepashchuk 1986). There are velocity shifts with the 13-day orbital period, described in early work by Crampton & Hutchings (1981), but they found that the shifts in H_β and He II λ4686 had different amplitudes and phases. Given the phase of the photometric light curve, the He II λ4686 line probably originates close to the compact object. Recently, D'Odorico et al. (1991) have found that different parts of this line show a different amplitude of Doppler modulation. The value for the centroid of the line, $K = 112 \pm 5\,\mathrm{km\,s^{-1}}$, combined with X-ray data (e.g.Kawai et al. 1989, Zwitter & Calvani 1989), would suggest that the compact object in SS433 is a neutron star.

It is widely accepted that the unique moving lines are emitted by matter moving at velocities of 0.26c in anti-parallel jets. The lines shift periodically in wavelength because the direction of ejection undergoes precession (the so-called 164-day motion). Superimposed on this long-term variation is a ~6-day nodding motion. Recent values of the parameters in this kinematic model are given by Margon & Anderson (1989). Moving Balmer, Paschen, and Bracket lines have been reported, as well as shifted He I lines (particularly λ 5876), but no shifted He II λ4686.

In this paper, the variability of both the moving and the stationary lines is analysed, with particular emphasis on H_α. An overview of the database and the reduction procedures is given in Sect. 2. Section 3 is devoted to an analysis of the evolution of the moving lines on timescales of hours. In Sect. 4 the variability of the stationary lines is addressed. Section 5 deals with spectrophotometric confirmation of a flare detected in broad band photometry. Section 6 is a summary of the results.

2. Observations and data reduction

Ten different telescopes were involved in the observing campaign. Because of the longitude distribution of the observatories and the other programmes they were following, there is somewhat of a twice-daily pattern, with denser intermediate coverage in the interval 0.5 to 1.0 of each Julian Day than in the other half. Details of all 202 spectra are given in Table 1. The wavelength coverage is non-uniform; the red region of the spectrum, containing the stationary and blueshifted H_α lines, was deliberately observed most often. The spectral resolution of the contributing instruments varied between 0.5 and 10 Å. The spectra are not all shown individually here. They are available to interested readers in digital form (FITS format) from the authors. A grey-scale representation of the complete database in the wavelength ranges of the moving H_α lines is given in Fig. 1. Time increases horizontally to the right in these grey scale figures, and wavelength vertically upward. Blacker portions indicate more intense emission. To construct these plots, each normalised spectrum (see below) was first placed into the frame as a vertical line at the appropriate time coordinate; tick marks at the upper margin of the diagrams indicate these locations. Then, the temporal evolution was filled up independently at each wavelength coordinate by linear interpolation between adjacent spectra along the time axis. This interpolation procedure was not used for further analysis; it was applied only to obtain solidly filled diagrams, which are very useful to display the overall characteristics of the database.

The data were combined in Leiden. Convolution to a common resolution was impractical and undesirable. Except where indicated, the original resolution and binning were preserved to be able to study whatever detail was available. Correction for the instrumental wavelength response curve and absolute flux calibration were attempted only by some observers. In order to allow a proper comparison, the spectra were all normalised. A flat continuum at an arbitrary value of 1 was enforced by fitting a smoothly varying (cubic spline) function to the continuum in the original spectra.

In the 13.081 day binary orbital cycle, primary photometric eclipses were predicted to occur at JD 2446936.36 and 49.45 (parameters given by Kemp et al. 1986). The first eclipse was indeed observed in the V-band by Aslanov et al. (1993), and in X-rays by Kawai et al. (1989). Due to these eclipses and to the flaring in the continuum (Aslanov et al. 1993, see also Sect. 5) the measured line fluxes (equivalent widths) had to be put on a common scale before their evolution could be studied. The V-band photometry of Aslanov et al. (1993) was used for this purpose. The time coverage of their observations is inhomogeneous. Typically, clusters of measurements are present at daily intervals, each consisting of up to 20 values at intervals of a few minutes. For each cluster of values, the weighted average was determined, and linear interpolation between these (nearly) daily values was then used to calculate V-band magnitudes appropriate for the time of observation of each spectrum. All equivalent widths were rescaled to a V-band magnitude of 13.9. This is close to the average "quiescent" magnitude outside eclipse; consequently, most correction factors were small. Although photometry is available to rescale most spectra, there were no measurements on JD 2446938, 46, 48–50, and 52–57; unfortunately the primary eclipse near JD 2446949 was missed. These gaps in the measured V-band data have been filled in from the *predicted* light curve, taken from Aslanov et al. (1993); the curve is shown in Sect. 5 as part of Fig. 11. This approach will, of course, lead to scaling errors if the true brightness of SS 433 deviated significantly from the long-term prediction, as happened, for instance, during the optical flare around JD 2446941.

3. The moving emission lines

Throughout this work, blueshifted lines will be indicated with a minus sign, and redshifted lines with a plus sign (e.g. H_α^- and H_α^+). This uniquely identifies the two jets at this precession phase, since the Doppler shifted lines were predicted to reach their largest separation in the 162.50 day precession cycle a fortnight before the start of our observations, at JD 2446919.3 (five-parameter model, see Margon & Anderson 1989). Defining that phase as $\psi = 0$, this database extends from $\psi = 0.094$ to $\psi = 0.238$.

Section 3.1 is an overview of the moving lines which have been detected. The main aim in obtaining this spectral database was a detailed study of the evolution of the shifted Balmer lines. There are 112 spectra near H_α^-, 53 around H_α^+, 75 covering H_β^+, and comparatively few on other members of the Balmer series. Some He I lines have been detected frequently (see Sect. 3.1), but at a much lower signal-to-noise ratio than the moving H_α lines. Since there are no indications for qualitative differences in the properties and evolution of different moving lines from one jet, we concentrate on H_α^- and H_α^+, the brightest lines, except in Sect. 3.1. A global description of the evolution of the moving

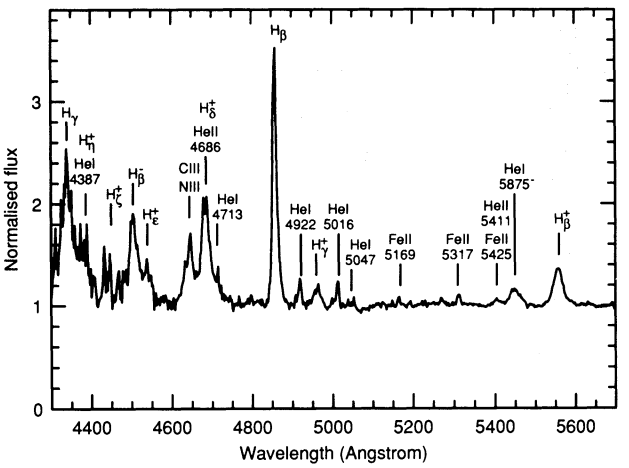

Fig. 2. Spectrum obtained on JD 2446945.605 at the Calar Alto 2.2 m telescope. It shows a number of Doppler shifted Balmer and He I lines, listed in section 3.1, as well as many stationary Balmer, He I, He II, and Fe II lines

lines is given in Sect. 3.2. In Sect. 3.3 it is first argued that this evolution is strongly indicative of the presence of bullets, and different observable properties are then analysed on the basis of gaussian profile fits. In Sect. 3.4 inferences from our results on the physical properties of the jets are discussed.

3.1. Occurrence of lines

The following moving Balmer lines have been detected in at least one spectrum: H_α^-, H_α^+, H_β^-, H_β^+, H_γ^-, H_γ^+, H_δ^+, H_ϵ^+, and H_ζ^+. The higher members mentioned can be seen nicely in Fig. 2. Bluer lines than those listed above have not been detected with certainty, due to the strong reddening of the spectrum of SS 433 and because relatively few spectra were obtained in the appropriate wavelength region.

The three strongest stationary He I lines are $\lambda\lambda$ 5876, 6678, and 7065. Of their moving counterparts, He I $\lambda 5876^-$ is usually clearly present (e.g. Fig. 2). He I $\lambda 5876^+$ is often blended with other lines, but has occasionally been detected unambiguously. The same is true for He I $\lambda 7065^-$. The sensitivity and resolution of the spectra is insufficient to establish the occurrence of He I $\lambda 7065^+$. Both moving He I $\lambda 6678$ lines are hard to distinguish from remnants of moving H_α; only the presence of He I $\lambda 6678^-$ has been established with confidence. Since the moving He I lines are broad, rather weak, and often blended with other spectral features, their equivalent widths have not been determined to high accuracy. The different moving lines may well have the same relative intensities as the stationary lines; this holds both between different moving He I lines, and between moving H_α and He I lines.

It is important to obtain limits on the occurrence of shifted He II $\lambda 4686$, since this constrains the excitation state (temperature) of the relativistically moving matter (e.g. Begelman et al. 1980, Davidson & McCray 1980). Unfortunately, any shifted He II $\lambda 4686$ emission would probably be wide, complex, and variable, like the Balmer and He I lines. Such lines are harder to find than narrower features. He II $\lambda 4686^+$ was not detected in any of the 72 spectra (on 21 days) in the appropriate wavelength range. Coverage of He II $\lambda 4686^-$ was much poorer. We estimate that a line at a normalised peak strength of 1.15 would have been detected in any of the spectra (where 1 is the continuum level). Many spectra allow peaks of strength 1.05 to be distinguished. The most stringent limit on He II $\lambda 4686^+$ can be derived from the spectrum shown in Fig. 2, which has a signal-to-noise ratio in excess of 100 in the appropriate wavelength region. We have also searched for He II $\lambda 4686^+$ by adding all 72 spectra, each shifted by an appropriate amount in velocity, given by the simultaneously observed Doppler shift of H_α^+ or H_β^+. The line could not be detected. However, this sum spectrum was somewhat confusing, due to differences in the resolution of the individual spectra. Furthermore, the noise of the sum spectrum was dominated by the many (variable) stationary lines (specifically of Fe II) which often overlap with He II $\lambda 4686^+$. This makes it especially hard to search for broad, complex features. We conclude that future more stringent limits, or detections, would be easiest to achieve by obtaining single spectra of very high signal-to-noise ratio.

Between 7700 Å (the atmospheric A-band) and 8200 Å (the Paschen limit in the stationary line system) many spectra show evidence for the presence of blueshifted Paschen lines, from $P11^-$ up to at least $P18^-$. The one spectrum which extends above 9500 Å has a signal-to-noise ratio which is too poor to detect any redshifted Paschen lines. The moving Paschen lines often appear to be very broad. Furthermore, for $P16^-$ and higher members, the day-to-day jumps in the wavelengths of the lines are often larger than the spacing between the lines, which makes it rather difficult to disentangle the lines whenever more than one line component ("bullet", see below) is visible. A detailed study of the moving Paschen line system was not attempted.

Interestingly, there is evidence that $P14^-$ is weaker than $P13^-$ and $P15^-$, though we cannot rule out that this is due to blending of $P13^-$ and $P15^-$ with shifted Ca II triplet lines ($\lambda 8662^-$ and $\lambda 8542^-$ respectively). The data quality was insufficient to verify this by comparing the equivalent width of higher members of the Paschen series. Filippenko et al. (1988) have previously reported the occurrence of blueshifted Paschen lines, blended with stationary lines, and often very broad, in agreement with our data. They mention $P12^-$, $P13^-$, and $P15^-$, but claim that blending was too severe to detect $P14^-$. However, we point out that on night 1 of their observations the predicted wavelength of $P14^-$ is fully clear of stationary lines. The line should also be distinguishable on their night 3; in fact, we believe that there is indeed a weak feature visible in Fig. 3 of Filippenko et al. (1988). We believe that their dataset supports the idea that $P14^-$ is weaker than $P13^-$ and $P15^-$. It would be useful to obtain a series of spectra specifically designed to investigate the strength and width of the moving Paschen lines. Unusual line ratios, or possible differences between the Balmer and Paschen line widths, or indeed the discovery of shifted Ca II lines, may hold important information concerning the collimation, fragmentation, and excitation of the jets of SS 433.

3.2. Overview of the evolution in H_α^- and H_α^+

Compilations of all the spectra in the shifted H_α regions are shown in Fig. 1. The overall trend in wavelength shows part of the precession cycle: the lines were moving towards lower radial velocities ($\psi = 0.094$ to $\psi = 0.238$), having reached their largest separation at $\psi = 0$ a fortnight before the start of our observations, according to the kinematic model prediction. The nodding motion stands out clearly. However, the variations are usually not smooth; rather, there are abrupt events, and dramatic changes from one night to the next dominate the database. The coverage is frequent enough to follow changes from hour to hour on several occasions. There are many instances of "bullet-like" phenomena: emission peaks emerge and decay at a particular wavelength; they do not shift as they evolve (*cf.* Grandi & Stone, 1982). This is clearly illustrated by the most rapid change of line strength which occurred in this database, displayed in Fig. 3. Near JD 2446940.9, 51.5, 53.5, and 56.5 the strength of the moving lines is greatly reduced; this phenomenon will be discussed in Sect. 3.3.6. We stress that neither the discrete behaviour, nor the occasional disappearance of the moving lines, are due to sampling problems, to smoothing, or to the interpolation applied in Fig. 1.

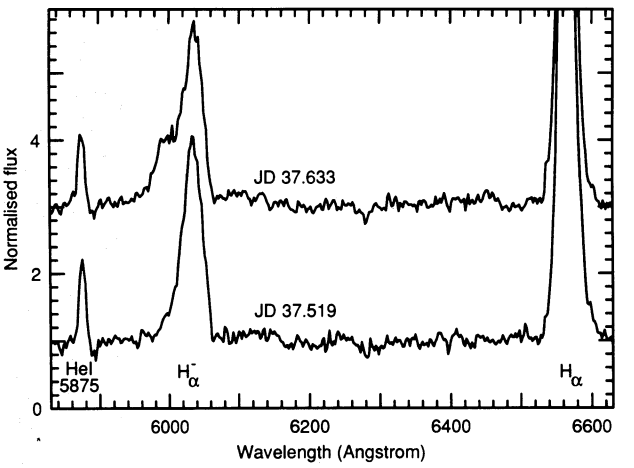

Fig. 3. The most rapid change of the H_α^- line profile found in the database. The spectra, shown with a normalised intensity offset of 2.0, were obtained within 3 hours of each other at the Calar Alto 1.2 m telescope (bottom: JD 2446937.519, top: 37.633)

3.3. Bullet analysis

3.3.1. The presence of bullets

The moving H_α line profiles are usually quite complex. If the database is divided into 48 successive intervals of 0.5 days, then spectra around H_α^- are available in 35 intervals. No H_α^- line could be detected in 2 of these (JD 2446951.5 and 56.5, see also Sect. 3.3.6). The H_α^- line has more than one separately visible peak in 25 out of 35 intervals. Despite the frequent multiplicity, one peak usually dominates. In 22 of the 35 intervals the amplitude of the highest peak in H_α^- is at least twice that of any other feature. This number includes the 8 intervals in which H_α^- shows only a single peak. However, in these 8 cases, the profile is usually asymmetric, suggesting that here, too, more than one component is present.

The frequent presence of multiple peaks in the shifted line profiles strongly confirms the idea that the Doppler shifted lines arise in "bullets" (well-defined moving entities), and not in a continuous flow. Moreover, it indicates that the bullets usually, though not always, appear at shorter time intervals than their total radiative lifetime (see Sect. 3.3.6). On occasion, two distinct line components from one jet arise and evolve almost simultaneously. Single but asymmetric line profiles may be explained by blended contributions from bullets with nearly the same projected velocity, but with unequal intensities. This view is supported by the bullet-like evolution of such line profiles over hours or days, which occurs in this database in several cases (see Sect. 3.3.5).

It is useful to investigate the properties of individual bullets under the assumption that each complex moving line profile consists of one or more gaussian components, each of these due to a single bullet. While in reality the line profile due to a specific bullet need not be gaussian, the parameters discussed below can be regarded as rough but manageable indicators of the properties of the bullets in the jets of SS 433. The underlying continuum of the spectra was forced to be flat, at an arbitrary value of 1 (see Sect. 2). Hence, the central wavelength (i.e. the Doppler shift), the Full Width at Half Maximum (FWHM), and the peak intensity (amplitude) of each gaussian remain as free parameters in a non-linear least-squares fitting algorithm. In the case of very weak lines which are broad, the FWHM and the peak intensity, which together define the equivalent width, unfortunately become dependent parameters; a large range of values is allowed, and the fitting is easily led astray by noise in the continuum. Some of these weak line profiles also do not seem to be very well described by a gaussian. In some cases, an upper limit on the FWHM (usually 3000 km s^{-1}) was imposed after visual inspection. The accuracy of the fits is of course also rather dependent on the signal-to-noise ratio in the continuum, and somewhat on the spectral resolution. Further errors were introduced in some cases by the necessity (obvious from Fig. 1) to remove atmospheric and interstellar absorption bands. This was achieved by interactively scaling templates obtained from spectra taken with the same instrumental setup on other nights. As very conservative overall margins for this database, we estimate that the peak intensities are accurate to ± 0.15 units, the FWHM to ± 200 km s^{-1}, and the positions to ± 3 Å (radial velocities to ± 150 km s^{-1}).

Initially, all profiles were fitted independently, and in each spectrum gaussians were added one by one up to the smallest number needed for a satisfactory fit. In many cases it could readily be seen in individual spectra or from Fig. 1 that weak remnant features were present for several days, and yet the preliminary results did not always allow us to follow the variations of such specific bullets. This is due to the fact that gaussian profile fitting has no unique solutions in the case of weak, blended components. Therefore, the gaussian analysis was repeated, the second time forcing the computer programme to find gaussian compo-

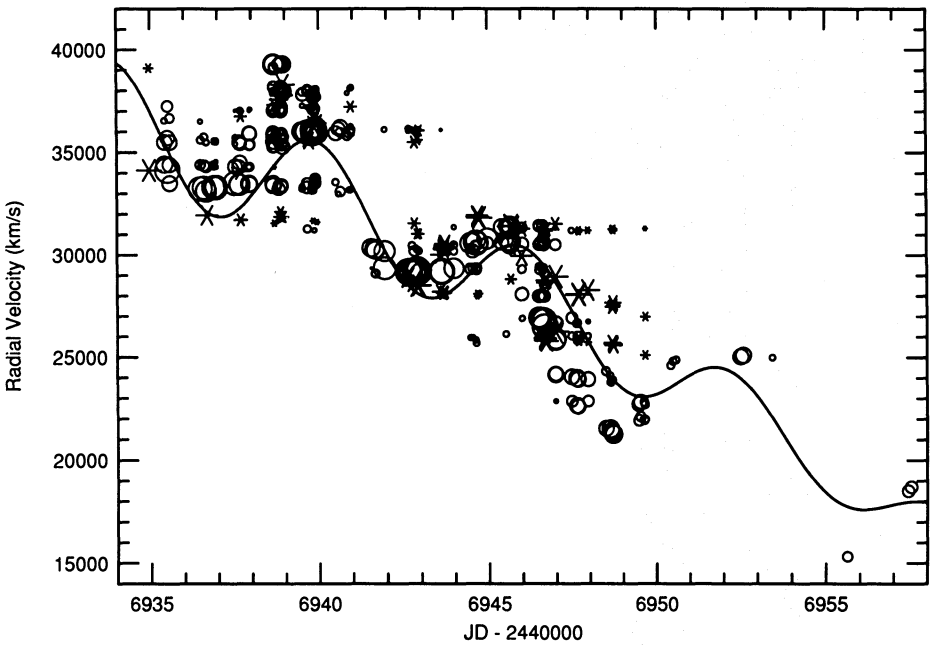

Fig. 4. Radial velocities of H_α^- (circles) and H_α^+ (stars), obtained by fitting gaussians to the spectral lines (see text). The surface area of each symbol is proportional to the equivalent width of the line. In order to compare both jets, the absolute value of the radial velocity is shown, after compensation for the transverse Doppler effect (see Sect. 3.3.2). The solid line represents the prediction of the kinematic model, including nodding motion

nents in certain fixed locations, given by the results of the original analysis and guided by visual inspection of the spectra. This decomposition occasionally had more gaussian components in a spectrum than the minimum number needed for a good fit, but we are confident that the final results provide the best overall fit to the database given the requirement of a consistent evolution. The analysis has resulted in the identification of 28 separate bullets in H_α^-, and 26 in H_α^+. Their properties will now be discussed. No firm one-to-one correspondences have been found between H_α^- and H_α^+ bullets (see Sect. 3.3.2 and 3.4.1). Therefore, comparisons of the gaussian profile parameters between the two jets must be based on their statistical distributions.

3.3.2. Radial velocity

The radial velocities of all fitted H_α^- and H_α^+ profiles are shown in Fig. 4, along with the kinematic model prediction: the 5-parameter precession model of Margon & Anderson (1989), with the nodding motion of Katz et al. (1982). In order to be able to compare the results of both jets, the transverse Doppler effect was removed, by computing the radial velocities relative to $\gamma\,\lambda(H_\alpha) \approx 6797$ Å rather than relative to H_α at rest. Figure 4 illustrates that individual H_α^- and H_α^+ bullets are not at all well correlated on a one-to-one basis. On the other hand, there is no evidence for systematic offsets in radial velocity between the two jets.

Overall, the predictions of the kinematic model are remarkably accurate. However, while the kinematic model is the framework for the Doppler shifts, individual bullets may have a projected velocity which differs by as much as 5000 km s^{-1} from the prediction. Short-lived deviations of the magnitude seen in our dataset are known to occur rather often; this phenomenon has previously been termed jitter (e.g. Margon & Anderson 1989). There is no evidence for any unusual offsets from the predicted curve. The overall (precession) trend was towards lower velocities. As a result of the presence of remnant emission ("old bullets"), there is a bias in both jets for the occurrence of larger radial velocities. Figure 4 shows that most of the time, the bullet with the greatest equivalent width (coded by surface area) tends to be closest to the predicted radial velocity curve, in agreement with the expectation that the kinematic model parameters largely reflect the Doppler shift of bullets at their peak strength. Yet, even most of the strongest bullets are either on the high velocity side of the predicted curve, or very close to it. A notable exception can be seen on JD 2446946 in both jets, and on the next three days in H_α^- only. We believe that little physical significance should be attached to the fact that most of the jitter happened to be towards higher projected velocities.

3.3.3. Line width

Figure 5 shows the distribution of line widths (full width at half maximum, FWHM), derived from fitting gaussians to the H_α^- and H_α^+ bullet profiles at the time they reach their maximum *observed* strength. The FWHM has a mean value and standard deviation of 1406±512 km s^{-1} for H_α^-, and 2024±707 km s^{-1} for H_α^+. The distributions have a tail extending out to >3000 km s^{-1}, and so the mean values quoted above are somewhat larger than the median values, which are 1314 km s^{-1} for H_α^- and 1917 km s^{-1} for H_α^+. Some of the high values in the tail of the distributions are rather uncertain, since they are from quite weak lines, or, in H_α^+, from profiles affected by the atmospheric A-band. Mostly, but not invariably, the moving line profiles are smooth on velocity scales below $\sim$ 1000 km s^{-1}, and the typical values found for the FWHM are certainly not an artefact of the spectral resolution.

There is no consistent pattern in the evolution of the FWHM as the bullets age. Some lines seem to broaden, but the FWHM of others decreases. Pronounced changes, if they occur at all, are seen only in the final stages, when the lines are very faint; the

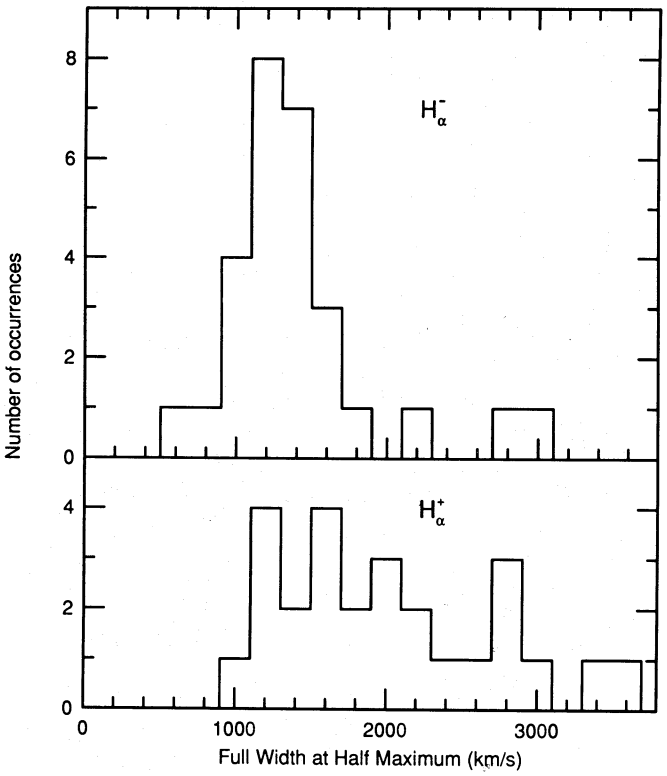

Fig. 5. The distribution of FWHM line widths in H_α^- (top) and in H_α^+ (bottom). For each bullet, the width at the time of its maximum measured line strength has been used

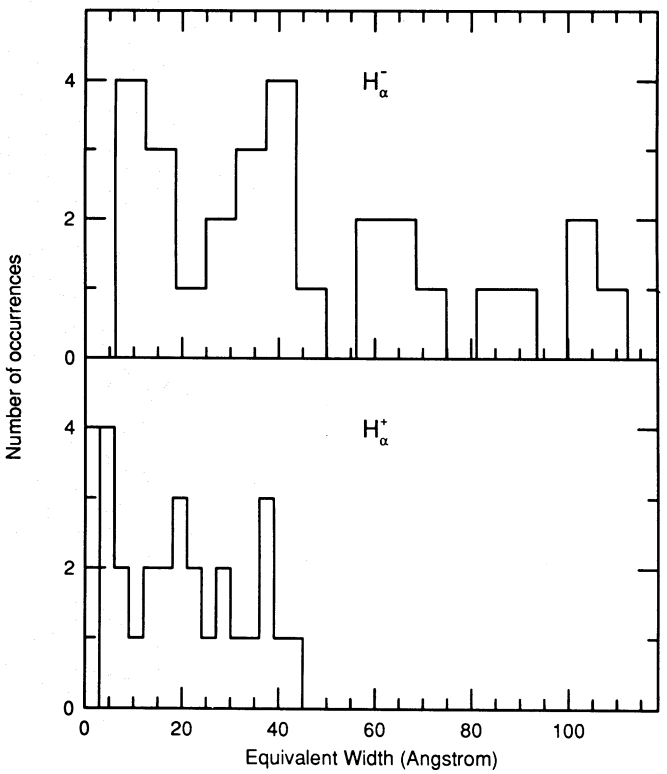

Fig. 6. The distribution of the largest observed equivalent width (W_λ) in each of the bullets of H_α^- (top) and H_α^+ (bottom), all corrected to a fiducial wavelength of 6797 Å (as explained in Sect. 3.3.4). Note that the widths of the H_α^- and H_α^+ bins are different by a factor of 2.08; this is explained in Sect. 3.3.4

fitting procedure is not very accurate in such cases. The data are consistent with most lines having a constant FWHM throughout their radiative lifetime.

While there are no definite one-to-one correspondences between bullets in the two jets, the H_α^+ lines are broader than the H_α^- lines by a factor of 1.44 (1.46), based on the mean (median) values; note that the standard deviation of the mean also scales. H_α^- and H_α^+ can also be compared by matching the cumulative distributions in the two jets, that is, by finding the multiplication factor for the H_α^- FWHMs which minimises the area between the two curves. This yields a ratio of 1.46. Milgrom et al. (1982) have previously established the existence of variations of the full width at zero intensity (FWZI) in data covering several precession cycles. Their model, which assumes that the two jets intrinsically have the same properties, predicts a typical ratio of ~1.3 between the FWZI in H_α^- and H_α^+ for our database. This agrees well with the ratio of ~1.45 determined for the FWHM distributions, given that there is a considerable spread in individual values. Hence, a typical intrinsic FWHM for our database is $\sim 1700\,\mathrm{km\,s^{-1}}$. This may well be indicative of the projected velocity spread within each bullet, and would agree with the relative velocity spread in each jet of $\leq 4\,10^{-2}$, or $\leq 3100\,\mathrm{km\,s^{-1}}$, in the best-fit model of Milgrom et al. (1982).

3.3.4. Maximum equivalent width

The distribution of equivalent widths (W_λ), measured for each bullet at the time of its maximum *observed* strength, is shown in Fig. 6; note the different bin widths used for H_α^- and H_α^+ (explained below). The equivalent widths within each jet can be compared directly, as they have been corrected for the eclipses and flares in the continuum (see Sect. 2). However, given the significant wavelength difference between H_α^- and H_α^+, the line strengths can only be compared between the two jets after a correction has been made from the enforced flat continuum to its intrinsic spectral shape. In the spectral region of interest a Rayleigh-Jeans law ($\propto \lambda^{-4}$) is a reasonable approximation to the intrinsic shape (e.g. Murdin et al. 1980, Wagner 1986), and for the purpose of converting equivalent widths measured at different wavelengths to a given fiducial wavelength, the precise value of the effective temperature can be ignored. The fiducial wavelength was chosen to be $\gamma\,\lambda(H_\alpha) \approx 6797$ Å, which has the advantage that it allows consistent values to be found throughout the precession cycle, with no correction needed during crossover of the lines. Typical scale factors were ~1.5 for H_α^-, and ~0.67 for H_α^+. Such factors have been applied for all equivalent widths shown in Figs. 6 and 7, and for all values quoted below.

As already stated, no unambiguous "bullet pairs" have been found, for which the equivalent width in H_α^- and H_α^+ could

be directly compared. After having been put on the same flux scale, H_α^- bullets are typically rather stronger than H_α^+ bullets. In the case of *optically thin* emission from matter moving at an angle θ to the line of sight, the total line flux is $\propto \delta^4$, where $\delta = \gamma(1 - \beta\cos\theta)$. For our database, θ of the approaching jet was typically $\sim 67°$, but with considerable variations. This predicts a typical factor of $\sim$2.25 in the total line flux between anti-parallel jets moving at 0.26 c. To probe the actual flux ratio, the cumulative distributions for H_α^- and H_α^+ were constructed. These curves were then matched by finding the multiplication factor for H_α^+ which minimises the area between the two cumulative distribution curves. Use of the full curves yields a factor of 2.08, while a value of 2.15 is obtained by excluding the smallest equivalent widths (which may be biassed, as explained below). The distribution of equivalent widths in the two jets is therefore in very good agreement with the Doppler boosting ratio predicted for optically thin bullets. Hence, the bin widths for the H_α^- and H_α^+ distributions shown in Fig. 6 were chosen to be different by a factor of 2.08.

Due to gaps in the monitoring, the highest observed line strengths are, of course, lower limits to the actual peak values reached by the bullets. In particular, we believe that this bias has led to an increased number of H_α^- bullets with maximum equivalent width $\leq$15 Å, and an increased number of H_α^+ bullets with maximum equivalent width $\leq$7 Å. The next peak in the distribution, at 35–40 Å for H_α^- and at 15–20 Å for H_α^+, on the other hand, probably reflects a true preferred maximum line strength for the bullets. However, rather brighter bullets occur regularly; the small number statistics agree with a gradually falling likelyhood. Asadullaev & Cherepashchuk (1986) have suggested that the strength of the Doppler shifted lines might vary with the orbital period. However, *after compensation for the continuum variations*, we find no obvious correlation of the equivalent width with the 13-day orbital period for our database. The pathlength travelled by the optically emitting matter ($\sim 10^{15}$ cm over its $\sim$ 2 day radiative lifetime, see Sect. 3.3.5) exceeds the plausible dimensions of the SS433 binary system by several orders of magnitude. It is therefore a priori quite unlikely that substantial variations with the orbital period would occur as a result of a changing amount of absorption.

Some of the brightest lines occur at the cusps in radial velocity of the nodding motion curve; this can be seen in Fig. 4. A similar effect has previously been noted by Kopylov et al. (1987). During the other extreme in the nodding cycle, when the radial velocity changes most rapidly, the moving line profiles show a range of properties. In some cases there is a rapid succession of rather weak lines, though distinct components can still be recognised. However, in other instances there are only a few line components, clearly separated. While the nodding motion geometry is certainly not the sole factor in determining the line strength, and perhaps not even the dominant factor, this phenomenon does suggest that some of the brightest lines are not, in fact, due to single physical entities, but, rather, that they are the effect of the superposition in projected velocity of the radiation from a rather long pathlength in the jets. This will be discussed in Sect. 3.4.2.

3.3.5. Curve of growth and decay

Individual bullets could be traced for periods between 0.5 and 6 days. Figure 7 shows the light curves of six bullets in H_α^- which were well monitored. The value plotted is the equivalent width, rescaled using broad-band photometry (see Sect. 2) and converted to a fiducial wavelength of 6797 Å (see Sect. 3.3.4). Coverage on the H_α^+ bullets was less extensive, but the information available agrees with the hypothesis that they display intrinsically similar evolution. Bullet-to-bullet variations in total lifetime are much larger than the possible slight longevity in H_α^+ compared to H_α^- predicted from light travel time effects.

For each bullet there seems to be only one maximum, after which the flux drops steadily. There could be a few instances in the database of bullets brightening late in their life, but these are more likely to be cases where a new bullet appears near the projected velocity of the first one. This view is supported by runs of the component fitting programme in which the component wavelengths were not held fixed; the fitted Doppler shift often jumps to a different value when there is a second brightening.

There are many clear instances of variations within half-an-hour in our database, and truly impressive changes in the line profile sometimes occur within three hours (e.g. Fig. 3). However, in all cases, the variability on such short timescales is due to, and forms part of, the rise and decline of bullets on slightly longer timescales. The shortest measured time taken by any bullet in the database to rise from being undetectably weak to reaching its maximum strength is 6 hours. While our database is much better suited to investigate this evolution than most previously published measurements, the predominantly twice-daily coverage is still not optimally matched to constrain it. For some bullets, only an upper limit to their rise time of 12 hours could be derived, but for others, rise times close to 24 hours were found. Overall, there seems to be a fairly narrow range of rise timescales. Of the bullets for which an actual value has been measured, none reaches its peak within 6 hours and none takes more than 24 hours. These values agree well with earlier estimates by Borisov & Fabrika (1987), based on models generated to match line profiles. A rise time of $\sim$10 hours may be typical. The shape of the rising part of the light curve is not accurately defined by our database; it could very well be largely linear. Unfortunately, a better determination is probably only possible by obtaining a long, rarely interrupted series of good signal-to-noise spectra at intervals of 3 hours around the clock.

The decline of the bullets occurs in one to several days. Hence, the fading part of the light curve is better defined than the brightening part. However, as can be seen in Fig. 7, the rate of decline varies from bullet to bullet. There is apparently no tightly defined fading law. A total radiative lifetime of $\sim$2 days, may be typical. The decay certainly does not take place linearly. There is some evidence in the light curves for a two-stage decline, with a fast initial drop to a low remnant level of emission which persists for a longer time. Given the increasing uncertainty in fitting weak features, this could also indicate an exponential fading law, as favoured by Borisov & Fabrika (1987). The longevity is correlated with the peak intensity reached: the

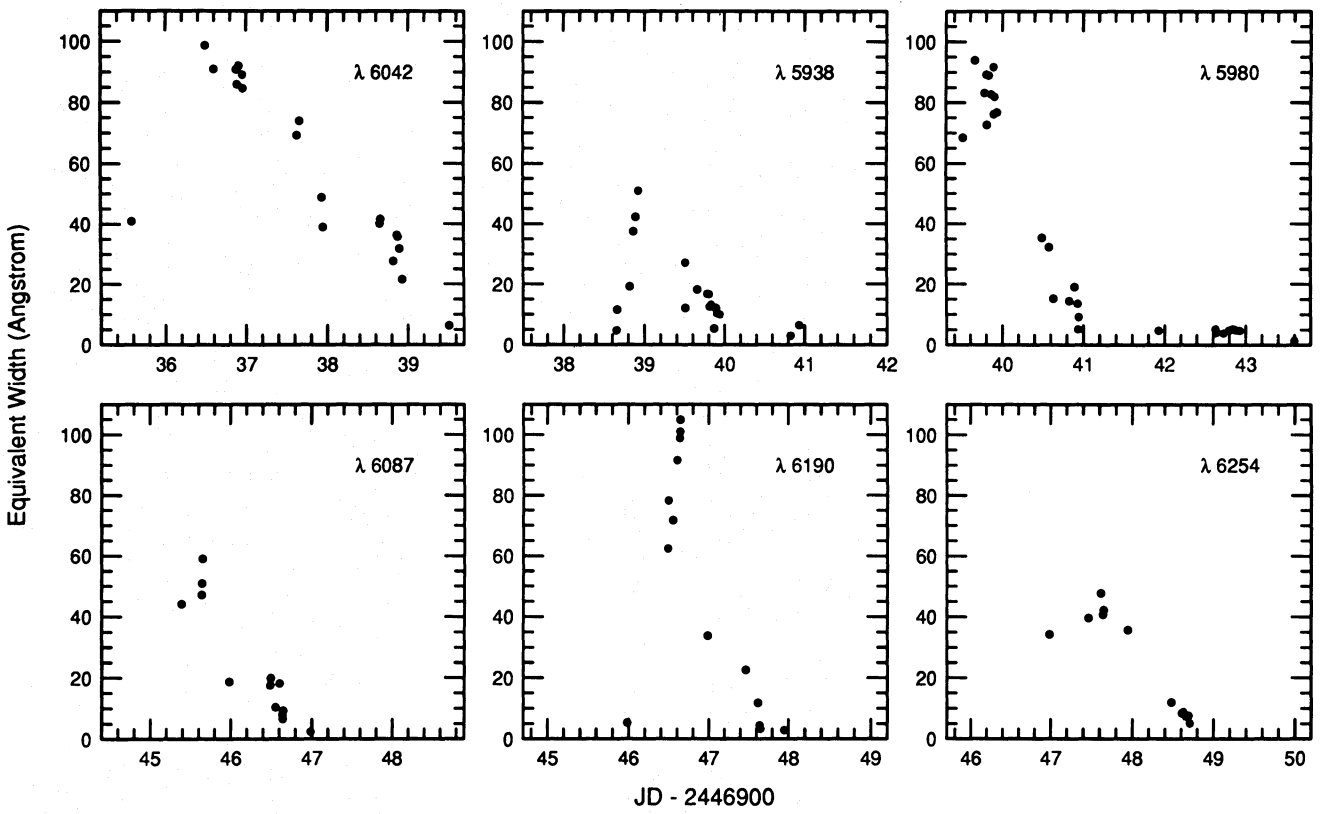

Fig. 7. Representative light curves (shown as W_λ) of some well-observed bullets in the H_α^- line system

longer-lived remnant emission tends to occur preferentially for brighter bullets. We believe that this phenomenon may be intrinsic and cannot be explained satisfactorily by a limited success in detecting weaker features.

3.3.6. Frequency of ejection; "switch-off" episodes

Unbroken daily coverage (or even more frequent monitoring) of both H_α^- and H_α^+ was obtained from JD 2446936.5–49.9. In that 13.4-day period, 20 H_α^- and 24 H_α^+ bullets were present, suggesting a mean ejection interval of ~0.6 days. The easiest point to study in the lifetime of the bullets is the time of maximum strength. The interval between the time successive bullets reach their maximum *observed* strength ranges from 0 to 2.14 days in H_α^-, and from 0 to 1.19 days in H_α^+; however, intervals >1 day are comparatively rare. The formal mean interval is 0.68±0.61 days in H_α^-, and 0.56±0.45 days in H_α^+. The formal errors should not be taken as an accurate representation of the intrinsic spread around the mean ejection interval, since they are affected by gaps (of <1 day) in the monitoring. However, bullet generation certainly does not occur with the regularity of a clockwork. Hence conclusions based on a model which assumes such regularity (e.g. Borisov & Fabrika 1987) will probably only have limited validity. Intervals between bullets much in excess of 1 day do not occur often. The typical radiative lifetime of each bullet is ≥1 day (Sect. 3.3.5), so that, indeed, more than one bullet can be distinguished at least 70% of the time (statistics given in Sect. 3.3.1). The data are entirely consistent with intrinsically equal average bullet generation rates in the two jets, but, as remarked before, there is no one-to-one correspondence of events.

The bullet generation rates found here are in agreement with the results of Grandi & Stone (1982). In early work, Margon et al. (1980) only rarely found instances of multiple line components. While it cannot be ruled out that the production rate of new bullets, or their lifetime, was somewhat different at that time, it is quite possible that multiple components were often missed due to the insufficiently dense time coverage of that earlier work. We are confident that in the central 14 days of our database all bullets have been identified and followed.

Only very faint remnants of the moving lines are visible around JD 2446940.9 and 53.5, while no lines are detectable around JD 2446951.5 and 56.5. This phenomenon clearly affects both jets, though for the period after JD 2446950 that conclusion is based on H_α^- and H_β^+, since no measurements of H_α^+ are available. Margon et al. (1984) were the first to describe instances when the moving lines of SS 433 could not be detected at all. This phenomenon is sometimes termed "switch-off", but this may carry a unnecessarily absolute connotation. For example, the periods around JD 2446940.9 and JD 2446953.5 in our database are only "near" switch-offs. We also suspect that in Figs. 2a and 2b of Margon et al. (1984) a faint H_α^- line is blended with the blue wing of stationary He I λ6678, while an equally faint H_α^+ line is blended with the blue wing of stationary He I λ7065. In the present paper, the moving lines are analysed

in terms of discrete line components, bullets, which appear at irregular intervals. At their peak strength the lines can usually easily be detected. A so-called switch-off will thus result when no new bullet appears within the time it takes for the last bullet to fade beyond detection. Therefore, the fundamental variables to study are the production rate of the bullets and their light curve. This description in terms of a discrete process (ejection of bullets) avoids the complicated issue of the occurrence of various "degrees of switch-off".

3.4. Discussion

3.4.1. Are the two jets connected?

It is obvious from Figs. 1 and 4 that the redshifted and blueshifted line systems are only partly correlated; this is borne out in the detailed analysis (Sect. 3.3). Frequently, a different number of bullets is visible in one jet than in the other, and there is no one-to-one correspondence between individual moving lines. In cases where there is one clearly dominant bullet in each jet, these bullets often have a different radial velocity. An offset in excess of 5000 km s^{-1} can be seen near JD 2446948. However, there are no indications for systematic offsets; we agree with earlier findings (e.g. Margon & Anderson 1989) that the best advance prediction of the Doppler shifts is obtained by using the same kinematic model parameters for both jets of SS 433.

The so-called switch-offs, periods of one to a few days when no new bullets can be detected, clearly affect both jets. Furthermore, though no clear-cut one-to-one correspondences have been found, there are occasionally individual features in the two jets which appear to have similar properties. Such lines are usually amongst the stronger ones, or amongst the ones which persist longest. However, this may be related to the fact that some of those strong lines occur at cusps in radial velocity due to the nodding motion; the correspondence may be geometric rather than physical.

The statistics derived from this database confirm that the two jets have bullets with similar properties. After compensation for relativistic effects, the radial velocities, the line widths, the line strengths, the light curves, and the rates of generation are all similar. We suggest that the two jets can be thought of as drawing bullets from the same statistical distribution. However, in some circumstances (extreme) events find their way into both jets. This applies in particular to the switch-offs, and perhaps also to some particularly long-lived bullets. Such extreme events may show the SS 433 "jet engine" when it is temporarily out of statistical equilibrium.

3.4.2. Bullets and pellets?

This database strongly reinforces the idea (e.g. Murdin et al. 1980) that the optical line emission in the jets of SS 433 is from discrete entities, moving ballistically, which have been called bullets. Most of the individual moving lines have quite similar properties. Typical or preferred values exist for the line width, the maximum total line flux and the time taken to reach that peak, and the generation interval between bullets. This suggests that the size-scale of the bullets can be reasonably tightly defined. On the other hand, there are occasionally features in the moving lines which are rather narrower. Also, there is a tendency for the brightest lines to occur when the nodding motion model predicts an accumulation of emission at the same radial velocity due to projection. This would suggest that bullets can occur on a range of size-scales.

Perhaps the jets of SS 433 should be visualized as consisting of a number of large clumps (called bullets in the above discussion), which are occasionally subdivided into smaller fragments (dubbed pellets by Vermeulen 1989). Weak but broad moving lines may be due to a number of these pellets, each at a different projected velocity, while in the brightest lines at the nodding motion cusps such entities may seen at the same projected velocity. This hypothesis has previously been pursued by Borisov & Fabrika (1987). Possibly, the typical width of the moving lines (1700 km s^{-1}) is representative of the projected velocity spread of pellets within a bullet. Occasionally visible narrow line features could be attributed to an individual pellet. However, many line profiles do not show such substructure. There is no significant difference in the FWHM of fainter and brighter bullets in this database, as could have been expected if they were composed of smaller separately moving pellets. Overall, the entities called bullets, which appear once or twice a day, seem to be the basic units from which the optical line emission originates.

It is important to note that neither the bullets, nor the occasionally visible smaller features (pellets), correspond to the clumps often invoked (e.g. by Begelman et al. 1980, Davidson & McCray 1980, Bodo et al. 1985) in order to obtain the observed H_α luminosity ($\sim 10^{35}$ erg/s) without requiring an implausibly large kinetic luminosity ($>10^{42}$ erg/s). The models discussed by Brinkmann et al. (1988) involve clumps with a radius of $\sim 10^8$ cm, and particle densities of $\sim 10^{14}$ cm^{-3}. In their simulations, the clumps are produced at a rate of $\sim 10^5$ per second. Hence, each bullet-like optical spectral line would originate from 10^9–10^{10} of these clumps. The jets could therefore still be considered smooth on the scales relevant for optical line emission (10^{14}–10^{15} cm) as long as the number density of the clumps does not vary too much.

3.4.3. Two-phase jets?

SS 433 is a source of thermal X-ray emission (e.g. Brinkmann et al. 1991), which is likely to originate in the inner $\sim 10^{12}$ cm of the jets. A steady outflow is indicated: the intensity measurements do not allow models in which there would only be outflow for, say, a few hours each day, corresponding to the hypothetical ejection of a bullet. Similarly, although there is certainly patchiness in radio maps on larger scales, Vermeulen et al. (1993a) have found that the core wing region in VLBI maps indicates smooth and continuous outflow with little substructure on scales $<10^{15}$ cm (i.e. little clumpiness on the scale of the optical bullets). Thus, no correlations exist between specific features in the VLBI maps of Vermeulen et al. (1993a) and specific optical

moving line components. However, the radio jets do adhere to the kinematic model with the same parameter values as derived from optical work; Vermeulen et al. (1993a) have even found evidence for the nodding motion in the VLBI maps. Several hypotheses can be considered to explain the apparent continuity of both the X-ray and the radio emission, and, in contrast, the intermittence of the optical moving lines, all from the same jets.

First, instabilities (bullets) could form in the jets at a distance of 10^{13}–10^{14} cm, and then disappear by the time the matter reaches $\sim 10^{15}$ cm. However, we do not know of a mechanism to achieve this; the length-scale as well as the time-scale for the generation and disappearance of the bullets may be uncomfortably tightly constrained.

Second, it is possible that the jet engine does not "swing" gradually, but points in a fixed direction for a number of hours, before suddenly shifting. This would generate elongated bullets. Of course, in this hypothesis the 6.7 keV Fe line in the X-ray spectrum should also show bullet-like radial velocity variations. However, these would not have been resolved in EXOSAT or Ginga spectra. If the outflow rate does not vary too much, either during or in between shifts in direction, then the X-ray intensity could remain constant, as required. However, while this would generate individual "chunks", a separate mechanism is still needed to explain why the integrated optical line strength is variable.

Third, the optical recombination lines could be due to another, differently distributed, particle population than the matter which gives rise to the X-ray and radio emission. Thus the optical bullets, of undetermined shape, would occupy only part of the volume of continuous jets. We believe this may be an attractive scenario. The jets could have a two-phase composition, with cool condensations (10^4 K) embedded in a hotter medium. Such a configuration has been investigated by Brinkmann et al. (1988) to fit X-ray data. However, their proposed clumps have a radius of $\sim 10^8$ cm, as already noted. The bullet-like optical recombination lines would then require modulations of some property of these clumps on a scale of $\sim 10^{14}$ cm, either their number density in the jets, or their mean internal density or temperature. Such variability could plausibly be related to slight changes in the initial conditions during the ejection from the central source, thus leading to a partial correlation between the two jets, as is required by the observations (Sect. 3.4.1).

It should be pointed out in passing that correlated variability between the two jets is more likely to be caused internally, by the jet engine, than by symmetrically encountering gradients in the ambient conditions, since these conditions are unlikely to change on timescales of a few days. For instance, while the wind flowing out from the SS 433 system is likely to be symmetric with respect to the jets, the jets "sample" the ejection history of the wind at a rate of >25 days per day even for a (high) assumed wind speed of $\sim 3000\,\mathrm{km\,s^{-1}}$.

It has long been recognised that the typical cooling timescales in the line emitting matter must be of order seconds to minutes. Hence an excitation mechanism is needed to obtain a radiative lifetime of a few days for each bullet. Furthermore, cooling of the bullets cannot set the timescale over which the bullets reach their peak brightness ($\sim$10 hours). Instead, this could simply be determined by geometry, either because it takes a number of hours to "eject" a complete bullet, or because it then takes a number of hours before all of the bullet has reached a minimum distance beyond which the excitation mechanism can operate.

In a recent study, Brown et al. (1991) favour shock excitation due to interaction with an ambient wind. A substantial fragmentation of the bullets (independently proposed on other grounds, as discussed above) would widen the otherwise rather tightly restricted allowed range in bullet size and mass. We also point out that there have been suggestions (e.g. Bodo et al. 1985) that the bullets may in fact stop radiating after a few days just because the small cool dense clumps in the jets have evaporated; this independent turn-off mechanism presumably would further alleviate the restrictions on the bullet properties found by Brown et al. (1991). Radiation beamed along the jets has been proposed as an alternative excitation mechanism for the optical lines (e.g. Fabrika & Borisov 1987). However, we feel that the geometric effects related to the swinging of both the physical jets and the light cone may be unable to explain the frequent simultaneous presence of multiple line components ("bullets"), the lack of detailed correlation between the two jets, the variable bullet generation rate, and the shape of the light curves.

Finally, the relatively small line width of the optical lines has often been cited as evidence for a collimation of the jets to better than $\sim 3°$. This agrees with the radio observations at larger radii, but those constraints are not very strong. However, the jitter in ejection angle shown by individual bullets could speculatively be interpreted to indicate that they occupy only a part of the cross-section of rather broader jets. Current X-ray spectroscopy, with limited resolution, does not constrain the jet collimation very tightly. In fact, recent work by Brinkmann et al. (1991) indicates that the Doppler shifted X-ray line is rather broad. While they favour an interpretation in terms of two separate emitting regions, we point out that, though rather speculative, an origin in a less well collimated jet should not be dismissed out of hand. Furthermore, Brinkmann et al. (1991) discuss a possible offset of part of the X-ray line profile from the Doppler shift predicted for matter moving at 0.26 c. We point out that the effect is towards the rest energy of the line at both precession phases discussed. This could speculatively be interpreted as being due to matter which has not yet been fully accelerated when it reaches $\sim 10^{12}$ cm. Note however, that studies of the jitter statistics over the precession period show that the optically radiating matter is indeed moving at 0.26 c (e.g. Anderson & Margon 1989). The ultimate constraints on the acceleration and collimation of the jets of SS 433 will therefore be derived from future high resolution X-ray spectroscopy.

4. The stationary emission lines

The stationary line profiles have structure on scales as small as $100\,\mathrm{km\,s^{-1}}$, in contrast to the moving lines, which are usually much smoother. Many of the spectra in the database do

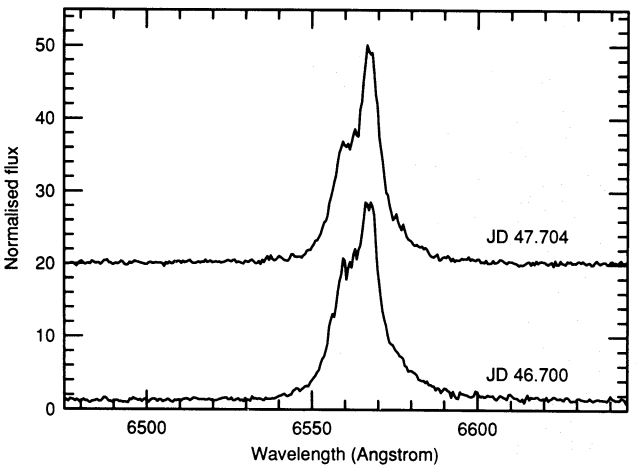

Fig. 8. Typical stationary H_α line profiles at high resolution. Different parts can be distinguished, as discussed in the text. The spectra were obtained one day apart at La Palma (JD 2446946.700 and 47.704)

not have the resolution required to study such features. Furthermore, the spectral coverage was not optimised to follow the evolution of any particular stationary line through the binary orbital period. Therefore no in-depth study of the stationary lines is presented here, and a detailed description of the evolution of He II λ4686, with a view to constraining the binary system parameters, was not attempted. However, some particularly intriguing profile variations of the stationary Balmer and Paschen series are discussed.

4.1. H_α line profile: shape and variability

Many more high resolution spectra are available covering H_α than on higher members of the Balmer series. While the following analysis is restricted to H_α, it was verified that H_β has similar properties as H_α.

Typical H_α line profiles at high resolution are shown in Fig. 8. The FWHM of H_α is typically 750 km s^{-1}, but it may exceed 1500 km s^{-1}. There are often sharp ($\sim$100 km s^{-1}) features. There is a bright central region and there are broad wings. The wings sometimes give the H_α line a total width (FWZI) of $\sim$3000 km s^{-1}. They are highly variable, in intensity as well as in maximum velocity extent. The red wing is usually brighter and more extended than the blue wing (but see below).

The central region is clearly subdivided into separate red and blue areas, as can be seen in Fig. 8. In this database the red part of the central structure is invariably the brightest side. Both parts have complex profiles; the "blue central feature", in particular, is too complex to be fitted with a gaussian component. The "red peak" is at a velocity of $\sim$ +190 km s^{-1} relative to the laboratory wavelength of H_α, as determined from the centroid of the few highest intensity pixels around the peak, in order to avoid contamination from other components. Significant systematic variations over the orbital period were not found in the velocity of the red peak; $K < 15$ km s^{-1} is a conservative upper limit to the amplitude of any Doppler modulation. Note that in previously published spectra of H_α (e.g. Margon et al. 1979, Murdin et al. 1980, Crampton & Hutchings 1981, Falomo et al. 1987), the brightest feature in stationary H_α is always very close in velocity to the brightest feature in our spectra, which we have termed the red peak. The blue central feature, while complex and hence not easily fitted, seems to be at a velocity of ~ -100 km s^{-1}, so that the separation between the two features is $\sim$300 km s^{-1}, and their mean velocity $\sim$+40 km s^{-1}.

All components of the profile vary on timescales well below one day; similarly rapid variations have been described before (e.g. Falomo et al. 1987). We have searched for correlated variability between stationary and moving H_α, in parameters such as line width or line strength. However, no unambiguously connected events or properties were found. For instance, the broad blue wing of H_α became much stronger on $\sim$JD 2446952, and it stayed rather strong for a few days. At about the same time, there were number of switch-offs of the moving lines (see Sect. 3.3.6). However, while the simultaneity is suggestive, it is not particularly well-defined in time. We are hesitant to regard this as a confirmed association of events. Broadening of the blue wing of H_α was not obvious during the earlier switch-off (JD 2446940.9).

After compensation for the broad-band light curve (see Sect. 2) no correlation of the total H_α line flux with the orbital period is apparent. However, during two separate time intervals, the total flux (equivalent width) of the blue central feature decreased very significantly; Fig. 8 documents such an event. While the red central peak is variable as well, no similarly drastic phenomenon was seen. The decrease in flux of the blue feature appears to be correlated with the eclipse of the accretion disk by the primary star in SS433 (at $\phi = 0$). While the data do not formally rule out that the decrease in intensity, which lasts $\sim$2–3 days, takes place symmetrically in time around the primary photometric eclipse, it is most likely that the phenomenon is phased $\sim$1 day ahead of the photometric eclipse. Unfortunately, the highest resolution spectra only cover the egress from one photometric primary eclipse (at JD 2446936.4) and the ingress into the next one (JD 2446949.4).

Confirmation of this phenomenon is available in independent data. Murdin et al. (1980) show a H_α profile obtained on September 8 1979, when $\phi \approx 0$; it resembles the upper spectrum in Fig. 8 quite well. We also believe that Falomo et al. (1987) registered similar eclipse events in their spectra. A primary photometric eclipse ($\phi = 0$) occurred exactly in the middle of their 3-night run. Given their tabulated parameters, we believe that the feature we have termed the "blue central feature" was significantly present only on their third observing night. In contrast, the component they label "blue peak" for their first two nights seems to be a much broader wing, similar to the additional blueward wing present in the spectra of Fig. 8. This seems to confirm that a decrease in brightness of the blue central feature takes place, phased somewhat ahead of the photometric eclipse cycle. Also in agreement with our data, there does not seem to be evidence for an eclipse of the red peak in the data of Falomo et al. (1987).

Figure 9 shows the radial velocity curve for the centroid of the H_α line. The entire profile was measured, including the broad wings; it was felt that any higher cutoff would be rather arbitrary.

While, as stated above, significant systematic variations over the orbital period were not found in the velocity of the red peak, in the line centroid there is clear evidence for orbital radial velocity variations. The outlying radial velocities towards the end of the measurements are due to a greatly increased brightness of the broad blue wing in the period JD 2446952–55. A sinusoid with a fixed period of 13.081 days (Kemp et al. 1986) was fitted to the early, well defined portion of the curve, JD 2446936–51 (see Fig. 9). This yielded a central wavelength of 6564.8 Å (+91 km s^{-1}), and an amplitude K = 0.66 Å (30 km s^{-1}). The maximum redshift occurs at photometric orbital phase ϕ = 0.81, (i.e. at JD 2446947.0 ± n 13.081). The errors in each of the centroid measurements cannot be quantified well, and we have not attempted to derive formal errors for the sinusoid fit.

It should be stressed that great caution is in order when using this curve (e.g. the K value) to derive information about the SS 433 binary system. Some seemingly outlying radial velocities (see Fig. 9) were ignored, indicating that both the K value and the central velocity based on what appears to be a regular curve over only a little more than one binary cycle, are open to considerable systematic error. The fact that the central velocity of the centroid curve (~+90 km s^{-1}) is to the red of the mean velocity of the two central features in H_α (~+40 km s^{-1}) is understandable given that the red peak is invariably the stronger of the two. The maximum radial velocity in the best-fit curve occurs at ϕ = 0.81, whereas, if the H_α line emission is postulated to be associated with the accretion disk (see Sect. 4.3), that should occur at ϕ = 0.75. This could be at least partly due to a shift introduced by the eclipse which seems to affect only the blue part of the profile. This 2–3 day event, which appears to be centered around $\phi \approx 0.92$ (see above), occurs rather close to the fitted phase of maximum redshift in the radial velocity curve of the H_α line centroid (ϕ = 0.81), and may have caused some skewedness in that curve.

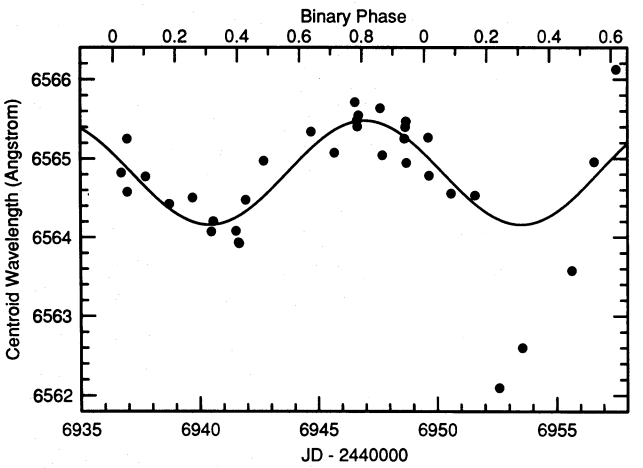

Fig. 9. Radial velocities of the centroid of the stationary H_α line. The entire profile, including the broad wings, was used to determine the centroid. The curve shown is the best-fit sinusoid in the period JD 2446936–51 (see Sect. 4.1)

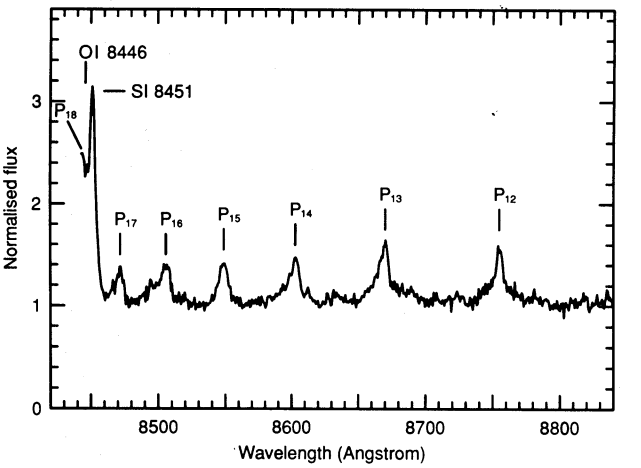

Fig. 10. High resolution near-IR spectrum showing the complex structure of the stationary Paschen line series. This spectrum was obtained on JD 2446949.697 at La Palma

4.2. Infrared spectra; Paschen lines

Only a few spectra were obtained in the near-infrared; the highest quality spectrum is shown in Fig. 10. The stationary Paschen series is clearly visible. Interestingly, these lines have features which are rather similar to the Balmer profiles in spectra obtained nearly simultaneously. The highest intensity is at a velocity consistent with that of the red peak in stationary H_α (~+185 km s^{-1}). The central part of the Paschen profiles is skewed, showing evidence for a second, lower brightness component to the blue; its separation from the red peak, while ill-defined, could well be ~300 km s^{-1}, as in H_α. In addition, there are broad wings; the red one being brighter and wider than the blue one, as is usually the case in H_α. Note that the spectrum shown in Fig. 10 was observed at orbital phase $\phi \approx 0$, when there was a substantial decrease in the brightness of the blue central feature in H_α. Since we find that in spectra observed nearly simultaneously the profiles of the Balmer and Paschen series have similar properties, we suggest that, in analogy with the Balmer lines, the blue side of the stationary Paschen line profiles may well have been stronger a few days earlier; the data quality unfortunately does not allow this to to be established unambiguously.

Earlier observations of the stationary Paschen lines have been presented by Filippenko et al. (1988); these were observed near orbital phase $\phi \approx 0.5$. The Paschen line profiles in Fig. 10 most closely resemble the profiles they found on their first observing night (see their Fig. 3). The velocity we find for the peak of the Paschen lines (~+185 km s^{-1}) is very close to that found by Filippenko et al. (1988) for their brightest (i.e. the "red") Paschen peaks, suggesting that this component shows little radial velocity variation over the orbital period. An additional blue peak in the Paschen lines, separated from the red feature by ~300 km s^{-1}, is most strongly visible in data taken by Filippenko et al. (1988) on their third night. As discussed above, there is evidence for this same component in our spectra, based on the skewedness of the line profiles, as well as on

the resemblance of the Paschen line profiles to simultaneously observed Balmer lines, which do show a brighter additional blue ($-100\,\mathrm{km\,s^{-1}}$) feature at other orbital phases.

A velocity of $\sim -100\,\mathrm{km\,s^{-1}}$ is also found in at least one other infra-red line: Ca II λ8927, again in confirmation of the result of Filippenko et al. (1988). In our spectra the blend of P18, O I λ8446 and S I λ8451 (indicated in Fig. 10) cannot be separated unambiguously, but it is compatible with a radial velocity in O I λ8446 of $-100\,\mathrm{km\,s^{-1}}$, especially if S I λ8451 is assumed to be quite a strong, sharp interstellar line.

4.3. Discussion

Early suggestions for a common or related origin of the stationary and moving emission lines due to interaction of outflowing matter in the jets with ambient matter (e.g. Begelman et al. 1980) now appear unlikely, given the lack of correlated variability between the stationary and moving lines, and given the abundant evidence for the influence of the binary system kinematics on the stationary line profiles. Unfortunately, this does not mean that there is now a consistent interpretation of the profiles in terms of the SS 433 binary system.

The Balmer and Paschen line profiles have strikingly similar features. The strongest component is generally at $\sim +190\,\mathrm{km\,s^{-1}}$. Tracking of this peak in our H_α spectra, and a comparison of our Paschen spectra to those of Filippenko et al. (1988), taken at opposite orbital phases, have revealed no significant systematic velocity variations over the orbital period. While this so-called red peak is variable in brightness, no obvious eclipse phenomenon has been revealed. In contrast, another, more complex, and generally more variable blueshifted feature, at $\sim -100\,\mathrm{km\,s^{-1}}$, does show a (partial) eclipse, which, in the Bal mer lines at least, may last for 2–3 days, centered $\sim$1 day before $\phi = 0$. Earlier data taken by Falomo et al. (1987) support these findings.

It was suggested by Filippenko et al. (1988) that the double-peaked Paschen lines, and similar features in several Fe II lines, could be indicative of Keplerian rotation in an accretion disk. However, this hypothesis matches neither the lack of significant orbital radial velocity variations in the red peak nor the fact that only the blueward part of the profile seems to undergo eclipses; a test Filippenko et al. (1988) had themselves indicated. It should be noted that $\sim -100\,\mathrm{km\,s^{-1}}$ is not only the velocity of the blue peaks in the Balmer and Paschen lines (and some Fe II lines, see Filippenko et al. 1988), but also the velocity of O I λ8446 and Ca II λ8927, without evidence for a shift during the binary orbital period. The most prominent feature in the hydrogen lines is always redshifted with respect to the line center, and the blueward part of the emission seems to be the most variable; as already pointed out by Murdin et al. (1980), this could well indicate an origin of the lines in an outflow. However, given that the radial velocity variations are small, either the true mass function of SS 433 is much smaller than hitherto assumed, or, more plausibly, the outflow is not localized very well near one of the orbiting bodies in the binary system. On the other hand, the phase of the (partial) eclipse of the blueshifted H_α feature suggests an occultation by the companion star or by matter flowing out from it, and hence a possible origin of that "blue" component, seen in many line species, in a wind flowing out from the accretion disk.

Though some line peaks show no clear evidence for orbital motion, the line centroid of H_α does. However, as explained in Sect. 4.1, additional variability may occur, and the radial velocity curve should be interpreted with caution. In early work, Crampton & Hutchings (1981) also discovered that the peak of H_β sometimes showed a regular radial velocity curve, but at other times only irregular variations (see also Kopylov et al. 1989). However, in view of differences in the resolution, it is not clear whether the radial velocity curve shown by Crampton & Hutchings (1981) would correspond only to the narrow feature we have called the red peak, or whether it reflects the velocity of a broader part of the line. The average velocity tabulated ($+223\,\mathrm{km\,s^{-1}}$) agrees reasonably well with the position of the red peak ($\sim +190\,\mathrm{km\,s^{-1}}$), but the Doppler amplitude ($K = 78\,\mathrm{km\,s^{-1}}$) is rather larger than that found here for the line centroid ($K \simeq 30\,\mathrm{km\,s^{-1}}$). In addition to this uncertain identification, however, there is a puzzling phase offset between the curves found by Crampton & Hutchings (1981) and Kopylov et al. (1989) (maximum redshift at primary photometric minimum, $\phi = 0.0$ in the phase convention of Kemp et al. 1986) and the curve found in our database (maximum redshift at $\phi = 0.81$).

It is also intriguing to compare our results on the Balmer and Paschen lines to recent work on He II λ4686. D'Odorico et al. (1991) have decomposed the complex profile of He II λ4686 into two components. As is the case for the hydrogen lines in our database, one of these components has a radial velocity curve which is much shallower than that of the line centroid. However, in the case of He II λ4686, this is the bluest peak, at a velocity of $\sim -190\,\mathrm{km\,s^{-1}}$ (the sign reversal with respect to the red peak in H_α is probably a numerical coincidence). The red peak in He II λ4686 is at a mean velocity of $\sim +300\,\mathrm{km\,s^{-1}}$, which implies a rather wider spacing ($\sim 500\,\mathrm{km\,s^{-1}}$) than in H_α, but yields the same average velocity between the two peaks: $\sim +40\,\mathrm{km\,s^{-1}}$.

Fabrika & Bychkova (1990), on the other hand, study the radial velocity curve obtained from the centroid of the upper part of the He II λ4686 line at times when its profile was relatively smooth and symmetrical. They find a central velocity near $0\,\mathrm{km\,s^{-1}}$, and a velocity amplitude of $134\pm21\,\mathrm{km\,s^{-1}}$. This agrees to within the errors both with the velocity amplitude found for the line centroid by D'Odorico et al. (1991), $112\pm5\,\mathrm{km\,s^{-1}}$, and with the value the latter authors obtained for the red peak, $133\pm24\,\mathrm{km\,s^{-1}}$. These values are all substantially higher than the value found for H_α in our database ($30\,\mathrm{km\,s^{-1}}$), but rather lower than the original measurement for He II λ4686 by Crampton & Hutchings (1981) ($195\pm19\,\mathrm{km\,s^{-1}}$). Intriguingly, however, a separate analysis by Fabrika & Bychkova (1990) of data around $\psi = 0$, when the disk is most inclined towards us, seems to indicate a curve with less scatter having a velocity amplitude of $175\pm20\,\mathrm{km\,s^{-1}}$. More work on the complex variability of the He II λ4686 line profile seems called for.

D'Odorico et al. (1991) do not discuss the fact that the radial velocity curve they find for the centroid of He II λ4686 is phased later by 0.1 than the result of Crampton & Hutchings (1981); based on the quoted uncertainties, the difference is highly significant. The curves derived by Fabrika & Bychkova (1990) are similarly phased as those of D'Odorico et al. (1991). It is very intriguing that those new He II λ4686 curves are nearly in phase with the curve for the centroid of H_α determined from our database. With new data for both H_α and He II λ4686, there is now apparently no longer a significant phase shift between the two line species.

In order to reconcile the phase of the He II λ4686 curve with the proposed origin of the line near the accretion disk, it may be necessary to appeal to a similar skewing mechanism due to a (partial) eclipse of the blue line component as can plausibly be invoked for H_α based on our data (see Sect. 4.1). Indeed, Fabrika & Bychkova (1990) suspected such an effect, though in their data, the effect of disregarding the suspected eclipse period was barely significant. D'Odorico et al. (1991) found that the relative intensities of the red and the blue He II λ4686 component vary over the orbital period. Their sinusoidal fit indicates that the blue component is weakest at $\phi = 0.94$. This is quite compatible with the eclipse event in H_α, for which we infer an offset of $\sim$1 day from $\phi = 0$. Note however, that, while D'Odorico et al. (1991) fit a sinusoid, the data in their Fig. 2b are sparse, and do not, we believe, contradict the conclusion from our H_α data that there is actually only an eclipse event which lasts 2–3 days, with superimposed random fluctuations. In He II λ4686, in contrast to H_α, the brightness of the two components seems to be more nearly equal on average.

In summary, a comparison of our results on the stationary hydrogen lines to older data and to recent work on He II λ4686 reveals intriguing similarities, but many puzzling aspects remain. Both the hydrogen lines and He II λ4686 have double peaks. By itself, the larger velocity separation between the main peaks in He II λ4686 than in the hydrogen lines matches well with an origin of these peaks in a rotating disk with a temperature gradient. However, while the components do change their brightness ratio during the binary period, the predicted eclipsing behaviour has not been found in H_α. Furthermore, in both lines the position of at least one of the peaks does not vary substantially over the orbital period. The centroids of both lines, on the other hand, do have a radial velocity curve, with the same phase, but with a rather different amplitude. The latter may suggest that at least part of the He II λ4686 emission is more narrowly localized near the compact object and accretion disk than the hydrogen emission. On the other hand, the central velocity in the radial velocity curve of the line centroid of He II λ4686, $\sim$+40 km s^{-1} (D'Odorico et al. 1991), is also the mean velocity of the two main components in both H_α and He II λ4686; and while the average velocity of the centroid of H_α is different ($\sim$+90 km s^{-1}), this may well be because, unlike in He II λ4686, the red peak in H_α is always brighter than the blue component. It is quite possible that the systemic velocity of SS 433 is close to +40 km s^{-1}. Thus the velocities of the two peaks in He II λ4686 and in H_α may reflect oppositely directed motion relative to the barycentre of the SS 433 system. All in all, it is likely that the overall line profiles arise in more than one emitting region and that the geometry is quite complex. While a contribution from a rotating disk is possible, and while part of the emission certainly seems to track the orbital motion of the compact object, other components seem to be due to a less localized outflow from the system. It is unclear whether any of the radial velocity amplitudes (K values) found to date accurately reflects the mass function of SS 433. There is also other evidence which suggests that the geometry of the binary system may be far from simple. It has long been thought that the accretion disk must be geometrically thick (e.g. Wagner 1986). Based on photometric observations, Zwitter et al. (1991) have suggested the presence of a disk-like outflow of matter. In order to explain recent X-ray data, Brinkmann et al. (1991) invoke both an extended (warped?) disk with large structures, and an X-ray scattering region at the base of the jets. Clearly, new, high resolution spectroscopy of the optical stationary line spectrum would be very desirable in order to elucidate the nature of the binary system.

5. Confirmation of a flare

This database was not compiled to be able to study the continuum of SS 433; only a few spectra are flux calibrated. However, it is worthwhile to use these spectra to confirm the occurrence of an optical flare around JD 2446941, as reported by Aslanov et al. (1993).

From each flux calibrated spectrum a V-band magnitude was derived by convolution with the bandpass of the V-band filter (Johnson 1965). The results are displayed in Fig. 11, with the V-band data and predictions of Aslanov et al. (1993) shown for comparison. Values obtained from different observatories, or in different spectral ranges, are shown with different symbols. There are some significant discrepancies between our spectrophotometric values, and the broad-band values of Aslanov et al. (1993). Equally, there are discrepancies between almost simultaneous values based on different spectra. Surely, part of the error is due to the uncertain extrapolation which was necessary for many spectra which do not span the full V-band. Note that most of the derived values are fainter than those of Aslanov et al. (1993); possibly, light losses have been underestimated when the spectra were calibrated.

In the relevant period, there were measurements at Flagstaff in two spectral ranges: 5520–8120 Å, and 3720–6340 Å. While there is an offset between the V-band magnitudes derived in the two spectral ranges, SS 433 was brightest in both sets during the measurements at $\sim$JD 2446940.9. These measurements were closest in time to the brightest broad-band values, at JD 2446941.4. The spectrophotometric values for the two preceding days are consistent with the observations of Aslanov et al. (1993): the flare started after JD 2446939.4. Since no flux calibrated spectra are available near JD 2446942, neither the decline of the flare nor the time at which the maximum actually occurred can be properly constrained, and a discussion of the magnitude of the flare is not warranted by the data.

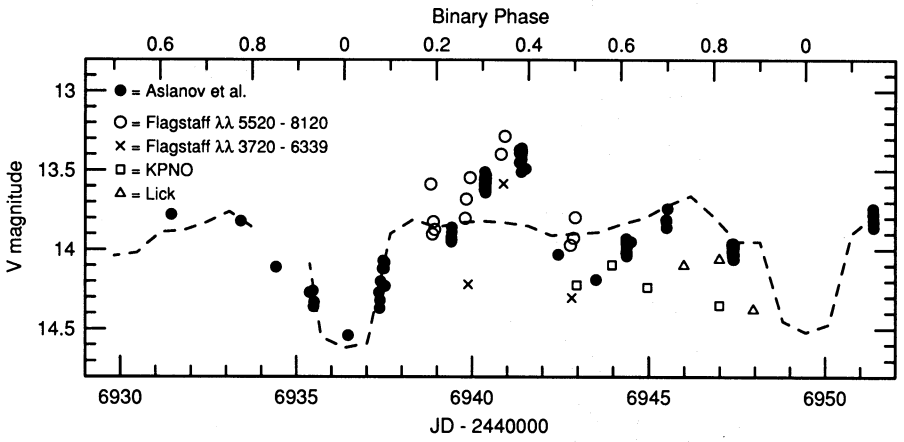

Fig. 11. Comparison between our spectrophotometrically determined V-band magnitudes (open symbols), and the broad-band photometry presented by Aslanov et al. (1993) (filled symbols, see also Fig. 1 in that paper). The dashed line has also been taken from Aslanov et al. (1993); it represents the magnitude predicted on the basis of the long-term behaviour of SS433

6. Summary

A unique database of 202 spectra was obtained over 23 days in May/June of 1987. This has enabled a study of the evolution of the moving lines of SS433 on timescales smaller than a day. It is clear that the moving lines consist of "bullets", discrete components which brighten and fade at a particular wavelength. A total of 28 H_α^- bullets and 26 H_α^+ bullets were studied by fitting gaussians to the line profiles. Their radial velocities show considerable "jitter" around the predictions of the kinematic model, but no systematic offsets. The ~6 day nodding motion stands out clearly. The lines are quite broad, and usually do not have much substructure. Their typical FWHM is $\sim 1400\,\mathrm{km\,s^{-1}}$ in H_α^- and $\sim 2000\,\mathrm{km\,s^{-1}}$ in H_α^+; this difference can be explained by orientation effects, and to first order, the bullets seem to have a typical intrinsic velocity spread of $\sim 1700\,\mathrm{km\,s^{-1}}$. The time taken by an individual bullet to reach its maximum brightness could typically be ~10 hours; no bullets have been observed to take either less than 6 hours or more than 24 hours to reach their peak strength. They then decay over one to several days, with a fast initial drop in strength and a slower fading of a low remnant level of emission. One bullet has been tracked for 6 days, but a total radiative lifetime of ~2 days may be typical. At their peak strength many H_α^- bullets have an equivalent width, corrected to a fiducial wavelength of 6797 Å, of 35–40 Å; many H_α^+ bullets reach a peak equivalent width of 15–20 Å corrected to the same fiducial wavelength. Bullets which are 2–3 times brighter occur regularly. The difference in brightness between the two jets is in good agreement with the Doppler boosting ratio expected for optically thin bullets. Some of the brightest lines occur at the cusps in radial velocity, suggesting that projection effects play a role, i.e. that not all "bullets" are single physical entities which have a fixed size. The bullets are typically generated at intervals somewhat shorter than one day. Occasional longer intervals lead to a so-called "switch-off" of the moving lines. While such extreme events are correlated between the two jets, there are no firm one-to-one connections between bullets. However, the statistical distribution of their properties is the same in both jets, after compensation for orientation effects. The clumpiness of the jets as seen in optical line emission and the more continuous outflow suggested by X-ray and radio emission can possibly be reconciled by having two-phase jets, with dense, cool clumps embedded in a more tenuous hot medium. The discrete optical lines may then arise as a result of a modulation of either the number density or the internal density of the cool clumps. These ideas remain rather tentative; a better understanding can be gained from future simultaneous X-ray and optical spectroscopy.

A comparison between our results on the stationary Balmer and Paschen lines, supported by older data, to recent work on He II λ4686, reveals intriguing similarities. The lines all have a double-peaked profile with broad wings. It is likely that emission from different locations contributes to those profiles. The velocity splitting in H_α is $\sim 300\,\mathrm{km\,s^{-1}}$, as opposed to $\sim 500\,\mathrm{km\,s^{-1}}$ in He II λ4686. The central velocity, $\sim +40\,\mathrm{km\,s^{-1}}$, may well be close to the systemic velocity of SS433. However, an interpretation in terms of Keplerian rotation in an accretion disk with a temperature gradient is thrown in doubt by the fact that no sequential eclipse of the two peaks is seen in the H_α lines, and the fact that in both line species at least one of the two peaks does not seem to exhibit the radial velocity curve expected due to orbital motion. Hence outflow with respect to the barycentre of the binary system may be partly responsible for the stationary emission lines. On the other hand, the blue peak in H_α, and possibly in He II λ4686, does show an eclipse which may be due to an occultation by the companion star or an outflow from it. Furthermore, the line centroids of H_α and He II λ4686 do show a radial velocity curve, phased as expected for an origin of the emission near the compact object. However, the Doppler amplitude was found to be $K \simeq 30\,\mathrm{km\,s^{-1}}$ in H_α, as opposed to $K = 112\,\mathrm{km\,s^{-1}}$ in He II λ4686 (D'Odorico et al. 1991). All values derived for the Doppler amplitude should be interpreted with great caution. Further high resolution spectroscopic monitoring of the stationary line spectrum could be expected to yield new insights into the dynamics of the binary system.

Acknowledgements. We are grateful to the directors and staff members at the ten observatories involved in our observations for their support. The Isaac Newton Telescope is operated by the Royal Greenwich Observatory, at the Spanish observatory of Roque de los Muchachos on La Palma, operated by the Instituto de Astrofisica de Canarias. The German-Spanish Astronomical Centre at Calar Alto is operated by the Max-Planck-Institut für Astronomie Heidelberg jointly with the Span-

ish National Commission for Astronomy. Parts of this work were done while one of us (RCV) was visiting the Royal Greenwich Observatory and the European Southern Observatory (ESO); he thanks these institutes for their hospitality. RCV was supported by the Netherlands Foundation for the Advancement of Research (NWO) through project 782-373-030; this paper was completed while RCV received support by the U.S. National Science Foundation under grant AST-9117100. The observations on La Palma took place on an override basis, and we are grateful to all observers who were affected by our programme. We thank R. Kennicutt, S. Anderson, and R. Cohen for obtaining some of the spectra, R. Blandford for a useful discussion, and the referee, M. Calvani, for his comments.

References

Anderson S.F., Margon B.H., Grandi S.A., 1983, ApJ 273, 697
Aslanov A.A., Cherepashchuk A.M., Goranskij V.P., Rakhimov V.Yu., Vermeulen R.C., 1993, A&A this issue
Asadullaev S.S., Cherepashchuk A.M., 1986, SvA 30, 57
Begelman M.C., Sarazin C.L., Hatchett S.P., McKee C.F., Arons J., 1980, ApJ 238, 722
Bodo G., Ferrari A., Massaglia S., Tsinganos K., 1985, A&A 149, 246
Borisov N.V., Fabrika S.N., 1987, SvA Lett 13, 200
Brinkmann W., Fink H.H., Massaglia S., Bodo G., Ferrari A., 1988, A&A 196, 313
Brinkmann W., Kawai N., Matsuoka M., Fink H.H., 1991, A&A 241, 112
Brown J.C., Cassinelli J.P., Collins II G.W., 1991, ApJ 378, 307
Crampton D., Hutchings J.B., 1981, ApJ 251, 604
Davidson K., McCray R., 1980, ApJ 241, 1082
D'Odorico S., Oosterloo T., Zwitter T., Calvani M., 1991, Nat 353, 329
Fabrika S.N., Borisov N.V., 1987, SvA Lett 13, 279
Fabrika S.N., Bychkova L.V., 1990, A&A 240, L5
Falomo R., Boksenberg A., Tanzi E.G., Tarenghi M., Treves A., 1987, MNRAS 224,, 323
Filippenko A.V., Romani R.W., Sargent W.L.W., Blandford R.D., 1988, AJ 96, 242
Grandi S.A., Stone,R.P.S., 1982, PASP 94, 80
Johnson H.L., 1965, ApJ 141, 923
Katz J.I., Anderson S.F., Margon B., Grandi S., 1982, ApJ 260, 780
Kawai N., Matsuoka M., Pan H.C., Stewart G.C., 1989,PASJ 41, 491
Kemp J.C., Henson G.D., Kraus D.J., Carroll L.C., Beardsley I.S., Takagishi K., Jugaku J., Matsuoka M., Leibowitz E.M., Mazeh T., Mendelson H., 1986, ApJ 305, 808
Kopylov I.M., Kumaigorodskaya R.N., Somov N.N., Somova T.A., Fabrika S.N., 1987, SvA 31, 410
Kopylov I.M., Bychkova L.V., Fabrika S.N., Kumaigorodskaya R.N., Somova T.A., 1989, SvA Lett 15, 474
Margon B., 1984, ARA&A 22, 507
Margon B., Anderson S.F., 1989, ApJ 347, 448
Margon B., Ford H.C., Katz J.I., Kwitter K.B., Ulrich R.K., Stone R.P.S., Klemola A., 1979, ApJ 230, L41
Margon B., Grandi S.A., Downes R.A., 1980, ApJ 241, 306
Margon B., Anderson S.F., Aller L.H., Downes R.A., Keyes C.D, 1984, ApJ 281, 313
Milgrom M., Anderson S.F., Margon B., 1982, ApJ 256, 222
Murdin P.G., Clark D.H., Martin P.G., 1980, MNRAS 193, 135
Vermeulen R.C., 1989, Ph.D. thesis, Univ. Leiden
Vermeulen R.C., Schilizzi R.T., Spencer R.E., Romney J.D., Fejes I., 1993a, A&A this issue
Vermeulen R.C., McAdam W.B., Trushkin S.A., Bonsignori-Facondi S.R., Fiedler R.L., Johnston K.J., Hjellming R.M., Corbin J., 1993b, A&A this issue
Wagner R.M., 1986, ApJ 308, 152
Zwitter T., Calvani M., 1989, MNRAS 236, 581
Zwitter T., Calvani M., D'Odorico S., 1991, A&A 251, 92

This article was processed by the author using Springer-Verlag TEX A&A macro package 1992.